

# Linear System Analysis and Optimal Control of Natural Gas Dynamics in Pipeline Networks

Luke S. Baker<sup>a,b,d</sup>, Sachin Shivakumar<sup>c</sup>, Dieter Armbruster<sup>d</sup>, Rodrigo B. Platte<sup>d</sup>, Anatoly Zlotnik<sup>a</sup>

<sup>a</sup>*Applied Mathematics & Plasma Physics, Los Alamos National Laboratory, Los Alamos, NM, U.S.A*

<sup>b</sup>*Center for Nonlinear Studies, Los Alamos National Laboratory, Los Alamos, NM, U.S.A*

<sup>c</sup>*School for Engineering of Matter, Transport and Energy, Arizona State University, Tempe, AZ, U.S.A.*

<sup>d</sup>*School of Mathematical and Statistical Sciences, Arizona State University, Tempe, AZ, U.S.A.*

---

## Abstract

We examine nonlinear and adaptive linear control systems that model compressor-actuated dynamics of natural gas flow in pipeline networks. A model-predictive controller (MPC) is developed for feedback control of compressor actions in which the internal optimization over the local time horizon is constrained by the dynamics of either the nonlinear system or the adaptive linear system. Stability of the local linear system is established and a rigorous bound on the error between the solutions of the nonlinear and linear systems is derived and used to devise situations when the linear MPC may be used instead of the nonlinear MPC without a significant difference between their respective predictions. We use several test networks to compare the performances of various controllers that involve nonlinear and adaptive linear models as well as moving-horizon and single-interval optimization. Our results demonstrate that the proposed moving-horizon MPC is well-equipped to adapt in local time to changes in system parameters and has the ability to reduce total computational costs by orders of magnitude relative to conventional transient optimization methods.

*Key words:* Model-predictive control, transient optimization, transfer function, linearization, eigenvalues, error analysis.

---

## 1 Introduction

Transient flows of natural gas in transmission pipelines are becoming more variable as a primary consequence of the use of gas-fired generators to compensate for load fluctuations cause by uncertain and intermittent renewable electricity production. Although steady-state optimization of compressor set-points remains fundamental for capacity analysis and planning [45, 34, 11, 31], predictive planning of day-ahead operations requires the optimization of transient flows [3, 49]. Algorithms are conventionally formulated for day-ahead planning in which the optimization is used to determine time-varying compressor control policies and flow schedules that can be used as a baseline for the subsequent 24-hour planning horizon. Early efforts to realize transient optimization

applied first order finite differences in space and time to the governing Euler equations or simplifications thereof [13, 40, 12, 27]. Pseudospectral methods [38] have been proposed more recently [50, 49] and have demonstrated the ability to estimate parameters [41] and facilitate coordination between natural gas and electric power systems [51]. On the other hand, model-predictive control (MPC) has been suggested for operating pipeline transients several decades ago and continues to gain interest [30, 1, 15, 2]. Because MPC is formulated as a feedback process, the internal transient optimization component of MPC is defined locally in time and may potentially be chosen to contain exactly the same number of decision variables as the steady-state problem. Therefore, in addition to adaptability and inherent robustness, MPC provides a computationally tractable approach to scaling transient control synthesis for operating a large gas pipeline network. Nonetheless, the nonlinearity, scale, and numerical ill-conditioning of the internal optimization program could still be challenging for contemporary computational methods. Linearization and model reduc-

---

*Email addresses:* [lsbaker@lanl.gov](mailto:lsbaker@lanl.gov) (Luke S. Baker), [sshivak8@asu.edu](mailto:sshivak8@asu.edu) (Sachin Shivakumar), [dieter@asu.edu](mailto:dieter@asu.edu) (Dieter Armbruster), [rplatte@asu.edu](mailto:rplatte@asu.edu) (Rodrigo B. Platte), [azlotnik@lanl.gov](mailto:azlotnik@lanl.gov) (Anatoly Zlotnik).

tion have emerged as viable tools to further reduce the computational complexity and increase the scalability of computational solutions to this problem [16, 9, 28, 14].

Mixed-integer linear and sequential quadratic programming were shown to yield feasible and physically meaningful solutions for the transient nonlinear optimization problem [12]. Linear programming constrained by linearized Euler equations has also been proposed [10], and a case study was used to showcase a reduction of computation time by two orders of magnitude in comparison to a nonlinear optimization program. On the other hand, linearization of the Euler equations and subsequent application of the Laplace transform offers a compelling alternative approach because it enables a closed-form representation of the transfer between input and output flow variables for connected networks of gas pipelines [46]. Padé approximations of the irrational transfer functions [25] followed by analytical inversion back to the time domain can also yield computationally efficient linear system realizations that have been used to estimate states [36, 4] and detect leaks in a pipeline [37]. Although pipeline field data has validated linear system modeling for certain transient flows [25, 5], recent pipeline simulations demonstrate that large changes in rates and amplitudes of flow variables may render linear modeling inapplicable [6, 7].

Our study makes two key contributions. The first is the formulation and rigorous error analysis of adaptive linear control systems that may be used to actuate the dynamics of natural gas flow in transmission pipelines. The above-mentioned transfer function representation is extended to analytically quantify restrictions on the amplitude and rate of change of the input variables within which the aforementioned simplifications of the Euler equations can be made. Next, a lumped-element discretization scheme for the simplified Euler equations is derived for general pipeline network topologies and the resulting finite-dimensional nonlinear control system is linearized about a nominal state to obtain a finite-dimensional linear system representation. Crucially, the nominal state can be steady or unsteady, which enables adaptive re-linearization about unsteady instantaneous states in predictive controller applications. Lyapunov methods are used to bound and characterize the error between the solutions of these finite-dimensional linear and nonlinear systems as a function of time and the magnitude of flow variation about the nominal state. Because this approach requires local input-to-state stability of the nonlinear system, we examine the eigenvalues of the local linear system. We prove that the local state evolution of the linearized system is asymptotically stable and derive a closed-form expression for the center of gravity of the eigenvalues.

The second key contribution of our study is the development of a moving-horizon model-predictive control (MH-MPC) synthesis for the transient optimization of compressor settings in natural gas pipeline operations. Our MH-MPC approach is formulated subject to nonlinear

and linearized dynamics to enable an online error analysis and a comparison to the analytically derived error bound mentioned above. Because the nominal state and local linear system are adaptively updated as time advances with the moving horizon, the derived error bound can be used to quantify the necessary frequency of the feedback controller with which the solution predicted by the adaptive linear system will remain accurate to within a specified error tolerance for all time. Although the proposed MH-MPC is adaptable to changes in system parameters and has provable performance metrics, we further highlight the practical significance of the MH-MPC by comparing its performance to one of the conventional transient optimization controllers [49, 8], which we refer to in the following as single-horizon optimal control (SHOC). In particular, numerical results for several test networks are used to examine the trade-off between the two controllers in terms of computation time, operational responsiveness, and total energy used for gas compression.

The remainder of the paper is outlined as follows. The PDEs and transfer function representation of gas flow in a pipeline are reviewed in Section 2 and an extension to an entire network is presented in Section 3. Section 4 reviews a lumped element discretization method and uses it to formulate a finite-dimensional approximation of the PDE system in terms of a system of ordinary differential equations (ODEs). The adaptive linear control system is derived in Section 5. Section 6 establishes several results pertaining to the eigenvalues of the finite-dimensional state matrix and their relation to the poles of the infinite-dimensional or irrational transfer matrix. Section 7 derives a rigorous bound on the error that may arise as a consequence to the local linearization of the flow dynamics in the network. The MH-MPC and the SHOC problem formulations are presented in Section 8 with which several computational studies are conducted thereafter in Section 9. Finally, a review of compelling future research directions is highlighted in Section 10.

## 2 Pipeline Flow Equations

The physics of natural gas flow through a horizontal pipe are approximated by the one-dimensional isothermal Euler equations [32, 33, 42],

$$\partial_t \rho + \partial_x(\rho v) = 0, \quad (1a)$$

$$\partial_t(\rho v) + \partial_x(\sigma^2 \rho + v^2 \rho) = -\frac{\lambda}{2D} \rho v |v|. \quad (1b)$$

The variables  $v(t, x)$  and  $\rho(t, x)$  represent the velocity and density of the gas, respectively, at time  $t \in [0, T]$  and axial location  $x \in [0, \ell]$ , where  $T$  denotes the time horizon, and  $\ell$  denotes the length of the pipe. The parameter  $\sigma$  represents the sound speed that is generally dependent on the temperature and pressure of the gas in accordance to equations of state. The above PDE system describes mass conservation (1a) and momentum conservation (1b). The Darcy-Weisbach term on the right-hand side of equation (1b) models momentum loss

caused by turbulent friction and is scaled by a dimensionless parameter  $\lambda$  called the friction factor. Restrictions on initial and boundary conditions under which the model in (1) is well-posed have been previously examined [18]. Because analytical solutions of the isothermal Euler equations exist only for certain cases of initial and boundary conditions [19], the solution must be obtained numerically for general systems and conditions. Initial and boundary conditions for general network topologies are described below.

### 2.1 Simplified Equations

The equation of state is approximated using the ideal gas law so that  $\sigma$  in equation (1b) is constant and uniform throughout the network. While non-ideal modeling may be necessary in practice to correctly quantify flows at pressures used in large gas pipelines, we suppose that ideal gas modeling allows qualitative description of the flow phenomena of interest. We further suppose that the gas velocity  $v$  is much lower than the sound speed  $\sigma$  so that the nonlinear term  $\partial_x(v^2\rho)$  may be removed from the momentum equation. Moreover, the inertia term  $\partial_t(\rho v)$  is omitted under the assumption of slowly-varying flows, resulting in the so-called friction-dominated PDE system [17]. These simplifications give rise to the flow equations

$$\partial_t\rho + \partial_x\varphi = 0, \quad (2a)$$

$$\delta\partial_t\varphi + \sigma^2\partial_x\rho = -\frac{\lambda}{2D}\frac{\varphi|\varphi|}{\rho}, \quad (2b)$$

where  $\varphi = \rho v$  is the cross-section mass flux. In the above equation, we include a binary parameter  $\delta$  with  $\delta = 1$  if the flux derivative term is included and  $\delta = 0$  otherwise. In the subsequent analysis, we consider both forms of simplified models and refer to the case in which  $\delta = 0$  as the friction-dominated approximation.

### 2.2 Transfer Matrix Analysis

Although numerical simulations indicate that the friction-dominated approximation for pipeline flow is applicable when the boundary conditions vary sufficiently slowly in time [32, 33], one of the potential drawbacks of using numerical simulations to predict the applicability of the friction-dominated approximation is that the results generally do not extend to changes in system parameters. In this section, we attempt to resolve this ambiguity by devising a method to quantify acceptable rates of changes in terms of pipeline parameters analytically. Because we are concerned with the response to time-varying boundary conditions, we assume that the pipeline variables are initially in a steady state. In a manner similar to the sinusoidal steady-state analysis of an electric circuit [25], our analysis is performed in the frequency domain using transfer functions [46, 6]. To obtain the transfer functions, the simplified models in equation (2) are linearized about the initial steady-state, the resulting space-varying coefficients are approximated using nominal constants, and the

Laplace transform is subsequently applied in time to the constant-coefficient linear PDEs.

Extending our previous study [6] from Fourier to Laplace transforms, the above operations formally result in the frequency domain representation

$$sP + \partial_x\Phi = 0, \quad (3a)$$

$$\delta s\Phi + \sigma^2\partial_xP = \alpha P - \beta\Phi, \quad (3b)$$

where  $s$  is the complex frequency and  $P(s, x)$  and  $\Phi(s, x)$  are the Laplace transforms of the variations of  $\rho(t, x)$  and  $\varphi(t, x)$ , respectively, about nominal steady-state values as functions of  $x$ . The true Jacobian coefficients are approximated with the constant parameters

$$\alpha = \frac{\lambda\bar{\varphi}|\bar{\varphi}|}{2D\bar{\rho}}, \quad \beta = \frac{\lambda|\bar{\varphi}|}{D\bar{\rho}}, \quad (4)$$

where  $\bar{\rho}$  and  $\bar{\varphi}$  are the constant baseline values of nominal density and steady-state mass flux, respectively. Field data [26] and simulations [6] indicate that the term involving  $\alpha$  in equation (3b) may be removed to further simplify the frequency domain representation without significant loss in accuracy. Effects of this additional simplification will be analyzed below in Figure 1. For ease of exposition, we denote inlet and outlet pipeline quantities using superscripts “0” and “ $\ell$ ”, respectively, e.g.,  $P^0(s) = P(s, 0)$  and  $P^\ell(s) = P(s, \ell)$ . Analogously to an electric circuit, we define series impedance  $z(s) = \delta s - \beta$  and the propagation factors  $\gamma_\pm(s) = \alpha/(2\sigma^2) \pm \gamma(s)$ , where  $\gamma(s) = \sqrt{\alpha^2/(4\sigma^4) + sz(s)}/\sigma^2$ . The solution of equations (3a)-(3b) evaluated at the ends of the pipe may be written in terms of these circuit quantities [6] as

$$P^\ell = \frac{\gamma_+e^{\gamma_+\ell} - \gamma_-e^{\gamma_-\ell}}{\gamma_+ - \gamma_-}P^0 - \frac{z}{\sigma^2} \frac{e^{\gamma_+\ell} - e^{\gamma_-\ell}}{\gamma_+ - \gamma_-}\Phi^0, \quad (5a)$$

$$\Phi^\ell = -s \frac{e^{\gamma_+\ell} - e^{\gamma_-\ell}}{\gamma_+ - \gamma_-}P^0 - \frac{\gamma_-e^{\gamma_+\ell} - \gamma_+e^{\gamma_-\ell}}{\gamma_+ - \gamma_-}\Phi^0. \quad (5b)$$

Two of the four inlet and outlet variables are specified as boundary conditions, while the remaining two variables represent the responses at the opposite ends of the pipe. For a single pipe, designated boundary conditions specify density at one end of the pipe and mass flux at the other end. By rearranging the above relations as a mapping from input to output variables, we obtain the transfer matrix representation given by

$$\begin{bmatrix} P^\ell \\ \Phi^\ell \end{bmatrix} = G \begin{bmatrix} P^0 \\ \Phi^0 \end{bmatrix}, \quad G(s) = \begin{bmatrix} G_{11}(s) & G_{12}(s) \\ G_{21}(s) & G_{22}(s) \end{bmatrix}, \quad (6)$$

where the coefficients of the  $2 \times 2$  transfer matrix  $G(s)$  are uniquely determined from the coefficients in equation (5). Under the further assumption that  $\alpha = 0$ , the transfer matrix simplifies to

$$G(s) = \begin{bmatrix} \operatorname{sech}(\ell\gamma(s)) & -\frac{z_c(s)}{\sigma} \tanh(\ell\gamma(s)) \\ \frac{\sigma}{z_c(s)} \tanh(\ell\gamma(s)) & \operatorname{sech}(\ell\gamma(s)) \end{bmatrix}, \quad (7)$$

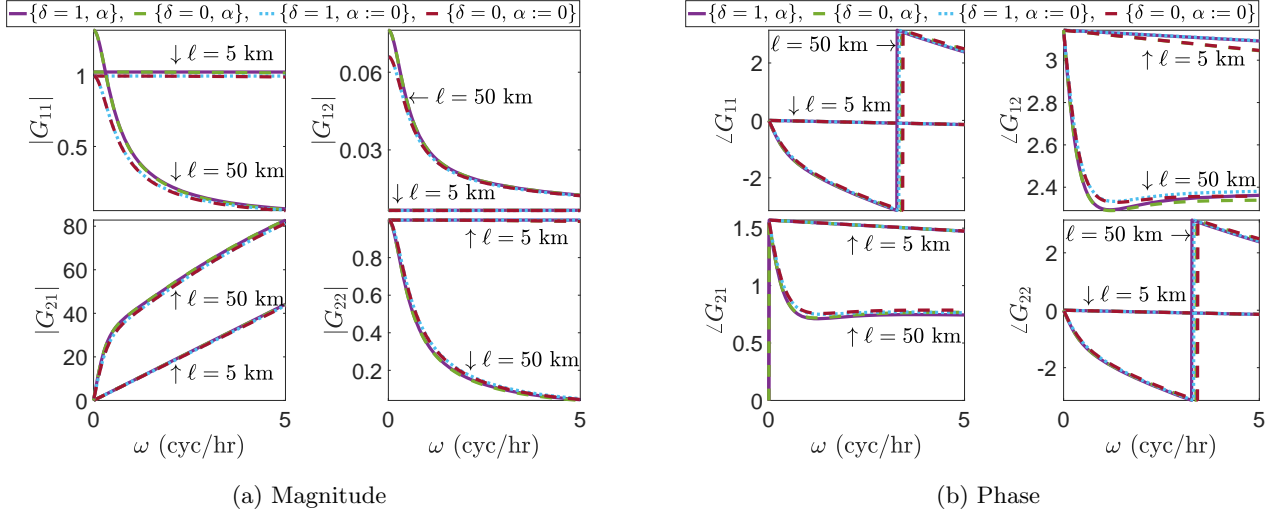


Fig. 1. Magnitude and phase of the transfer matrix coefficients for two pipes of lengths 5 km and 50 km, and the four linear models produced by the combinations of taking zero and nonzero values for  $\alpha$  and  $\delta$ , as indicated in each panel. The remaining parameters are  $D = 0.5$  m,  $\sigma = 377$  m/s, and  $\lambda = 0.011$ , with nominal values  $\bar{\varphi} = 300$  kg/sm<sup>2</sup> and  $\bar{p} = 35$  kg/m<sup>3</sup>.

where  $z_c(s) = \sqrt{z(s)/s}$ .

By evaluating equation (6) for each of the combinations of zero and nonzero values for  $\alpha$  and  $\delta$ , we obtain a collection of four linear systems. Loosely speaking, we suppose that the systems in this collection are approximately equivalent to one another if each system attenuates and delays the boundary condition variables in approximately the same way. To quantify rates of changes in boundary conditions for which the systems are approximately equivalent, we write  $G_{mn} = |G_{mn}|\angle G_{mn}$  and analyze the magnitude  $|G_{mn}|$  and phase  $\angle G_{mn}$  of  $G_{mn}$  as a function of frequency. As seen from the transfer matrix representation, the magnitudes of the coefficients attenuate the amplitudes of the input wave components to produce the amplitudes of the output wave components. The phases of the matrix coefficients introduce time delays between input and output. The magnitude of each frequency component  $\omega$  of an input wave is attenuated and delayed differently, in general, depending on the values of  $|G_{mn}(j\omega)|$  and  $\angle G_{mn}(j\omega)$ , respectively, in which  $s = j\omega$ , where  $j = \sqrt{-1}$  is the imaginary unit. Therefore, the simplified linear systems for all combinations of  $\alpha$  and  $\delta$  are approximately equivalent over a range of frequencies if the magnitudes and phases of the resulting transfer matrices are approximately equivalent over the range of frequencies under consideration. This argument may be quantified rigorously by specifying a threshold on the absolute difference between the magnitudes and phases of transfer matrix coefficients for any two of the linear systems and subsequently inverting the differences numerically to express the maximum frequency of the allowable range as a function of the chosen threshold. Here we approximate the suitable frequency ranges by visual inspection, as described below.

The magnitudes and phases of each transfer matrix coefficient are displayed in Figure 1 as functions of input frequency for each of the four linear systems. For fre-

quencies less than 5 cyc/hr, the magnitudes and phases of each coefficient are in excellent agreement for short pipes. For relatively long pipes, the magnitudes and phases of each coefficient are in agreement except for the magnitudes of  $G_{11}(j\omega)$  and  $G_{21}(j\omega)$  corresponding to the fully simplified model described by  $\delta = 0$  and  $\alpha = 0$ . However, because the magnitude of the coefficient  $G_{21}(j\omega)$  significantly increases as the frequency increases, the amplitude of the output flux wave will also significantly increase with increasing frequency of the input density. Such destabilization of the transfer function representation of gas pipeline flow was described in our previous study [6]. In that study, the nonlinear and linearized flow equations are simulated for a 100-km pipe with the same parameters as described in Figure 1 to show that varying the input density with a frequency of 8.33 cyc/hr can induce an inlet flux that varies in amplitude to a maximum of nearly 350% with respect to the steady-state flux. Because such extreme variations are prevented in practice, constant or nearly constant input pressure is usually a designated specification for simulations and pipeline practices [35]. In the absence of pressure variation about the steady-state, it follows that  $P^0 = 0$  and hence  $G_{11}$  and  $G_{21}$  have no effect on the output variables. Therefore, in the case of constant input density, all of the linear models are again in agreement for frequencies less than 5 cyc/hr. Based on the results shown in Figure 1, we conclude that any one of the four simplified models may generally be used to describe natural gas flow changes generated solely by variations in mass flux withdrawal if the frequency spectrum of variation is primarily less than 5 cyc/hr. We adhere to these restrictions in our subsequent analysis.

### 3 Network Flow Equations

We extend the flow equations from a single pipe to a representation in which gas flows through a network of

pipelines with an arbitrary topology. We begin by introducing some definitions. A pipeline network is modeled as a connected and directed graph  $(\mathcal{E}, \mathcal{V})$  consisting of a set of edges  $\mathcal{E} = \{1, \dots, E\}$  that represent pipelines and a set of nodes  $\mathcal{V} = \{1, 2, \dots, V\}$  that represent junctions or stations where gas is injected into or withdrawn from the network. Here,  $E$  and  $V$  denote the numbers of edges and nodes of the graph. The elements of the edge and node sets are ordered according to the ordering of the integer labels. The symbol  $k$  is reserved for indexing edges in  $\mathcal{E}$ , and the symbols  $i$  and  $j$  are reserved for indexing nodes in  $\mathcal{V}$ . The nodes of the network are partitioned into nonempty sets of supply nodes  $\mathcal{V}_s \subset \mathcal{V}$  and withdrawal nodes  $\mathcal{V}_w \subset \mathcal{V}$ . Supply and withdrawal nodes are ordered in  $\mathcal{V}$  so that  $i < j$  for all  $i \in \mathcal{V}_s$  and  $j \in \mathcal{V}_w$ . The graph is directed by assigning a positive flow direction along each edge with the convention that edges incident to supply nodes are directed away from them. Mass flux and velocity are positive quantities along a given edge if and only if gas physically flows along this edge in the prescribed orientation of the graph, and negative otherwise. The notation  $k : i \mapsto j$  means that edge  $k \in \mathcal{E}$  is directed from node  $i \in \mathcal{V}$  to node  $j \in \mathcal{V}$ . For each node  $j \in \mathcal{V}$ , we define (potentially empty) incoming and outgoing sets of pipelines by  $\mapsto j = \{k \in \mathcal{E} | k : i \mapsto j\}$  and  $j \mapsto = \{k \in \mathcal{E} | k : j \mapsto i\}$ , respectively. Here  $i \mapsto$  and  $\mapsto j$  each contain at least one edge for all  $i \in \mathcal{V}_s$  and  $j \in \mathcal{V}_w$ .

For each pipe  $k \in \mathcal{E}$ , the state variables are the cross-sectional density  $\rho_k(t, x)$  and the mass flux  $\varphi_k(t, x)$  for time  $t \in [0, T]$  and axial location  $x \in [0, \ell_k]$ , where  $\ell_k$  denotes the length of the pipe. As above, the flow of gas through the pipe indexed by  $k \in \mathcal{E}$  is governed by

$$\partial_t \rho_k + \partial_x \varphi_k = 0, \quad (8a)$$

$$\delta \partial_t \varphi_k + \sigma^2 \partial_x \rho_k = -\frac{\lambda_k}{2D_k} \frac{\varphi_k |\varphi_k|}{\rho_k}, \quad (8b)$$

where  $D_k$  and  $\lambda_k$  are the diameter and friction factor of the pipe, respectively, and  $\sigma$  is the sound speed. As in the previous section,  $\delta$  may be specified to be either zero or one if the magnitude of the power spectrum of variations in the boundary conditions is negligible for frequencies above 5 cyc/hr, as is the case in the typical operating regime of gas transmission pipelines.

We define  $\mathcal{C} \subset \mathcal{E}$  to be the set of edges  $k \in \mathcal{E}$  incident to a compressor station and simply refer to an edge  $k \in \mathcal{C}$  as a compressor. By bisecting an edge into two edges if necessary, we may assume that each compressor  $k \in \mathcal{C}$  is located at the inlet of its incident edge  $k \in \mathcal{E}$  with respect to the graph orientation. The action of the compressor  $k \in \mathcal{C}$  is modeled with the multiplicative control variable  $\mu_k(t)$  with  $1 \leq \mu_k(t)$  for all  $t \in [0, T]$ . In particular, the pressure of gas discharged from the compressor unit  $k \in \mathcal{C}$  is  $\mu_k(t)$  times larger than the suction pressure. To simplify notation, we define  $\mu_k = 1$  for all  $k \in \mathcal{E} \setminus \mathcal{C}$ .

Natural gas is injected into the network at supply nodes  $i \in \mathcal{V}_s$  with density  $\mathbf{s}_i(t)$  specified as a boundary condition. We allow for time-varying supply density in the

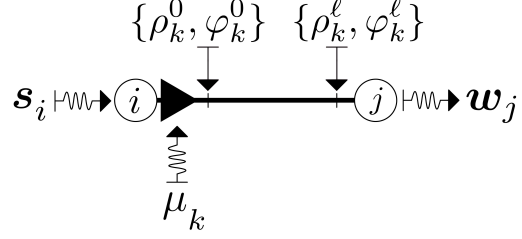


Fig. 2. Configuration of a pipeline segment  $k : i \mapsto j$  with  $i \in \mathcal{V}_s$  and  $j \in \mathcal{V}_w$ . Flow and control variables are indicated.

derivations that follow, but we emphasize that flows are generally simulated under constant supply density. Mass outflow from each withdrawal node  $j \in \mathcal{V}_w$  is specified as a boundary condition with the symbol  $\mathbf{w}_j(t)$ . All nodal quantities in this study are denoted using bold symbols. As with the input and output variables of the transfer matrix, we denote inlet and outlet edge variables using superscripts “0” and “ $\ell$ ”, respectively, e.g.,  $\varphi_k^0(t) = \varphi_k(t, 0)$  and  $\varphi_k^\ell(t) = \varphi_k(t, \ell_k)$ . Define  $\chi_k = \pi D_k^2/4$  to be the cross-sectional area of pipe  $k \in \mathcal{E}$ . The boundary conditions for gas flow in the network are

$$\rho_k(t, 0) = \mu_k(t) \mathbf{s}_i(t), \quad \rho_k(t, \ell_k) = \rho_j(t), \quad (9a)$$

$$\rho_k(t, 0) = \mu_k(t) \rho_i(t), \quad \rho_k(t, \ell_k) = \rho_j(t), \quad (9b)$$

$$\mathbf{w}_j(t) = \sum_{k \in \mapsto j} \chi_k \varphi_k^\ell(t) - \sum_{k \in j \mapsto} \chi_k \varphi_k^0(t), \quad (9c)$$

where equation (9a) is defined for  $k : i \mapsto j$  with  $i \in \mathcal{V}_s$ , equation (9b) is defined for  $k : i \mapsto j$  with  $i \in \mathcal{V}_w$ , and equation (9c) is defined for  $j \in \mathcal{V}_w$ . The conditions in equations (9a)-(9b) represent the effects of compression, and the conditions in equation (9c) represent the conservation of mass flow through withdrawal nodes. The initial condition throughout the network is defined by

$$\rho_k(0, x) = \varrho_k(x), \quad \varphi_k(0, x) = \phi_k(x), \quad \forall k \in \mathcal{E}, \quad (10)$$

where  $\varrho_k$  and  $\phi_k$  are consistent with the control and boundary condition variables for each  $k \in \mathcal{E}$ . The network flow equations are defined by the initial-boundary-value system of PDEs in equations (8)-(10).

#### 4 Lumped Element Discretization

The system of PDEs in equation (8) is discretized in space using a lumped element method [22] to obtain a system of ordinary differential equations (ODEs). Such spatial discretization over a graph is formalized as a refinement of the graph topology of the network. We create a *refinement*  $(\hat{\mathcal{E}}, \hat{\mathcal{V}})$  of the graph  $(\mathcal{E}, \mathcal{V})$  by adding auxiliary nodes, which are categorized as withdrawal nodes with zero outflow from the network, which partition the edges of  $\mathcal{E}$  so that  $\ell_k \leq \ell$  for all  $k \in \hat{\mathcal{E}}$ , where  $\ell$  is a specified limit on the lengths of the pipeline segments in the refined graph. For lumped element simulation of natural gas transport,  $5 \text{ km} \leq \ell \leq 10 \text{ km}$  has been verified empirically to be sufficiently fine discretization for simulations and field data experiments in the physical regime

of pipeline operations under usual conditions [16], [52]. The refined graph inherits the prescribed edge orientations of the parent graph. We suppose that the subsequent derivation is applied to the refined graph, and hat symbols associated with the refined graph node and edge sets will be omitted.

The system of ODEs is obtained by integrating the dynamic equations (8a)-(8b) along the length of each pipeline segment  $k \in \mathcal{E}$  so that

$$\int_0^{\ell_k} \partial_t \rho_k + \partial_x \varphi_k dx = 0, \quad (11a)$$

$$\int_0^{\ell_k} \delta \partial_t \varphi_k + \sigma^2 \partial_x \rho_k dx = -\frac{\lambda_k}{2D_k} \int_0^{\ell_k} \frac{\varphi_k |\varphi_k|}{\rho_k} dx. \quad (11b)$$

The above integrals of space derivatives are evaluated using the fundamental theorem of calculus. Following a previous study [22], the remaining integrals are evaluated by approximating the density variable over the refined segment with the density at the outlet of the refined segment and the flux variable over the refined segment with the flux at the inlet of the segment. Factoring the approximate integrand terms out of the integrals and incorporating the actions of the compressors in equations (9a)-(9b), we obtain the set of ODEs for each  $(k : i \mapsto j) \in \mathcal{E}$  given by

$$\ell_k \dot{\rho}_j = \varphi_k^0 - \varphi_k^\ell, \quad (12a)$$

$$\ell_k \delta \dot{\varphi}_k^0 + \sigma^2 (\rho_j - \mu_k \rho_i) = -\frac{\lambda_k \ell_k \varphi_k^0 |\varphi_k^0|}{2D_k \rho_j}, \quad (12b)$$

with slack node densities defined by  $\rho_i = \mathbf{s}_i$  if  $i \in \mathcal{V}_s$ . A dot above a variable will always represent the time-derivative of the variable. It remains to incorporate the boundary condition in equation (9c) by taking linear combinations of equation (12a) over the set of pipeline segments immediately entering a withdrawal node and collecting the resulting set of equations for each withdrawal node. Because the edge-node incidence matrix of the network graph may be used to express sums and differences of physical quantities at the ends of graph edges, in the following we utilize the incidence matrix as an alternative to linear combinations because it directly produces a system of ODEs in matrix-vector form.

Define the  $E \times E$  diagonal matrices  $L$ ,  $K$ , and  $X$  with diagonal entries  $L_{kk} = \ell_k$ ,  $K_{kk} = \lambda_k/(2D_k)$ , and  $X_{kk} = \chi_k$ . Define the weighted edge-node incidence matrix  $\Xi$  of size  $E \times V$  component-wise by

$$\Xi_{ki} = \begin{cases} -\mu_k(t), & \text{edge } k \in i \mapsto \text{leaves node } i, \\ 1, & \text{edge } k \in i \mapsto \text{enters node } i, \\ 0, & \text{else.} \end{cases} \quad (13)$$

The rows of  $\Xi$  correspond to the edges of the network and the columns correspond to the nodes. For each  $(k : i \mapsto j) \in \mathcal{E}$ , the  $k$ -th row of  $\Xi$  contains exactly two nonzero entries that appear in the  $i$ -th and  $j$ -th columns with values  $\Xi_{ki} = -\mu_k$  and  $\Xi_{kj} = 1$ . The matrix  $\Xi$  operates on a vector of nodal density values to produce a finite

difference approximation of its spatial derivative after compression. Define the  $E \times V_s$  submatrix  $N$  of  $\Xi$  by the selection of columns  $i \in \mathcal{V}_s$  and the  $E \times V_w$  submatrix  $M$  of  $\Xi$  by the selection of columns  $i \in \mathcal{V}_w$ , where  $V_s$  and  $V_w$  denote the numbers of supply and withdrawal nodes, respectively. The purpose of defining these submatrices is to separate the known nodal density variables at supply nodes from the unknown density variables at withdrawal nodes. Define the  $E \times V_w$  signed matrix  $Q = \text{sign}(M)$  componentwise with the convention that  $\text{sign}(0) = 0$ . The signed matrix is well-defined by the lower bound on the compressor variables. Define the positive and negative parts of  $Q$  by  $Q_\ell$  and  $Q_0$ , respectively, so that  $Q = (Q_\ell + Q_0)/2$  and  $|Q| = (Q_\ell - Q_0)/2$ , where  $|A|$  denotes the componentwise absolute value of a matrix  $A$ .

Define inlet and outlet edge mass flux vectors by  $\varphi^0 = (\varphi_1^0, \dots, \varphi_E^0)'$  and  $\varphi^\ell = (\varphi_1^\ell, \dots, \varphi_E^\ell)'$ . Define the vector of supply node densities  $\mathbf{s} = (\mathbf{s}_1, \dots, \mathbf{s}_{V_s})'$ , the vector of withdrawal node densities  $\boldsymbol{\rho} = (\boldsymbol{\rho}_{V_s+1}, \dots, \boldsymbol{\rho}_V)'$ , and the vector of withdrawal node outflows  $\mathbf{w} = (\mathbf{w}_{V_s+1}, \dots, \mathbf{w}_V)'$ , where the subscripts of the entries are indexed according to the node labels in  $\mathcal{V}$ . By applying the above matrix definitions, the discretized equations (12) together with the boundary conditions (9) can be written as a system of differential-algebraic equations (DAEs) of form

$$LQ_\ell \dot{\boldsymbol{\rho}} = \varphi^0 - \varphi^\ell, \quad (14a)$$

$$L\delta \dot{\varphi}^0 + \sigma^2 (M\boldsymbol{\rho} + N\mathbf{s}) = -LK \frac{\varphi^0 \odot |\varphi^0|}{Q_\ell \boldsymbol{\rho}}, \quad (14b)$$

$$\mathbf{w} = Q'_\ell X \varphi^\ell + Q'_0 X \varphi^0, \quad (14c)$$

where  $\odot$  denotes component-wise multiplication and the ratio of vectors on the right-hand side of equation (14b) is defined component-wise. Henceforth, the ratio of two vectors will always be used to denote component-wise division. As expected, we may observe upon substitution of the above matrix definitions into equations (14a)-(14b) for a given network structure and performing the multiplications that formulation (14a)-(14b) is equivalent to equations (12) for all  $k \in \mathcal{E}$ . Multiplying both sides of equation (14a) on the left by  $Q'_\ell X$  and using (14c), we obtain the equation  $Q'_\ell X LQ_\ell \dot{\boldsymbol{\rho}} = (Q'_\ell X \varphi^0 - \mathbf{w})$ , where we use the fact that  $Q = (Q_0 + Q_\ell)$ . Observe that the outlet flux becomes a dependent variable. Now, define the state vector of inlet flux by  $\varphi = \varphi^0$ . Proposition 1 below shows that the matrix  $\Lambda = Q'_\ell X LQ_\ell$  that pre-multiplies the time derivative of density is diagonal with positive diagonal components.

**Proposition 1** *The  $V_w \times V_w$  matrix  $\Lambda = (Q'_\ell X LQ_\ell)$  is diagonal with positive diagonal components*

$$\Lambda_{(j-V_s), (j-V_s)} = \sum_{k \in i \mapsto j} \chi_k \ell_k \quad (15)$$

for each  $j \in \mathcal{V}_w$ .

**Proof** First, suppose that  $j \in \mathcal{V}_w$  is the only withdrawal node in the network. Then  $Q_\ell$  and  $XLQ_\ell$  are

vectors with nonzero entries in the  $k$ -th rows if and only if  $k \in \rightarrow j$ . Thus,  $\Lambda = Q'_\ell(XLQ_\ell) = \sum_{k \in \rightarrow j} \chi_k \ell_k$  is a scalar. Now suppose  $\mathcal{V}_w$  contains two or more withdrawal nodes and consider  $i, j \in \mathcal{V}_w$ . If  $i \neq j$ , then the sets  $\rightarrow i$  and  $\rightarrow j$  are disjoint. Therefore, the column of  $Q_\ell$  corresponding to  $i \in \mathcal{V}_w$  and the column of  $(XLQ_\ell)$  corresponding to  $j \in \mathcal{V}_w$  are orthogonal, so that  $\Lambda_{(i-V_s), (j-V_s)} = \sum_{k \in \mathcal{E}} (Q'_\ell)_{ik} (XLQ_\ell)_{kj} = 0$ . If  $i = j$ , then again, the  $(j-V_s)$ -th columns of  $Q_\ell$  and  $XLQ_\ell$  have nonzero entries in the  $k$ -th rows if and only if  $k \in \rightarrow j$ , so

$$\Lambda_{(j-V_s), (j-V_s)} = \sum_{k \in \mathcal{E}} (Q'_\ell)_{ik} (XLQ_\ell)_{kj} = \sum_{k \in \rightarrow j} \chi_k \ell_k.$$

This completes the proof.  $\square$

A practical consequence of Proposition 1 is that the inverse of  $\Lambda$  may be obtained simply by inverting the diagonal components. Moreover, Proposition 1 implies that the  $(j - V_s)$ -th diagonal component of  $\Lambda$  may be interpreted as the total cylindrical volume of all refined pipeline segments directed to and incident to the withdrawal node  $j \in \mathcal{V}_w$ . The indexing shift by  $V_s$  is related to the node indexing of  $\mathcal{V}$  described above. By inverting  $\Lambda$ , the dynamical system of the pipeline network is written as

$$\dot{\boldsymbol{\rho}} = \Lambda^{-1} (Q'X\boldsymbol{\varphi} - \boldsymbol{w}), \quad (16a)$$

$$\delta\dot{\boldsymbol{\varphi}} = -\sigma^2 L^{-1} (M\boldsymbol{\rho} + N\boldsymbol{s}) - K \frac{\boldsymbol{\varphi} \odot |\boldsymbol{\varphi}|}{Q_\ell \bar{\boldsymbol{\rho}}}. \quad (16b)$$

The state vectors are withdrawal node density  $\boldsymbol{\rho}$  and edge inlet flux  $\boldsymbol{\varphi}$ . The compressor variables are contained in the matrices  $M$  and  $N$ . The other matrices are known and constant. The system (16) is numerically consistent in the sense that the discretized ODE dynamics approach the continuous dynamics (8)-(9) as the refined network edge length approaches zero [49]. The initial condition of the discretized system is equal to the sampled initial condition in equation (10) at the refined nodes and edges of the network, and is defined by

$$\boldsymbol{\rho}(0) = \boldsymbol{\rho}, \quad \boldsymbol{\varphi}(0) = \boldsymbol{\phi}. \quad (17)$$

## 5 Adaptive Linear Control System

Because it is possible that the nonlinear system in (16) may not be well-conditioned for large networks without appropriate preconditioning [39], we consider adaptive linear system approximations of the nonlinear dynamics. We suppose that such an approximation is made about a nominal state denoted by  $\bar{\boldsymbol{\rho}}$  and  $\bar{\boldsymbol{\varphi}}$ . This state is chosen to be consistent with nominal boundary condition values denoted by  $\bar{\boldsymbol{s}}$  and  $\bar{\boldsymbol{w}}$  together with nominal values for the compressor control variables or equivalently nominal values for the weighted incidence matrices  $\bar{M}$  and  $\bar{N}$ . In the following, a variable with a bar attached to it will always represent a nominal vector or matrix of the corresponding variable. The nominal state is defined to be a currently estimated state and not necessarily a steady state of the system. A linear model that governs the dynamics about an arbitrary nominal state provides the user

with flexibility to adaptively update the nominal state and linear system dynamics as time progresses to ensure applicability of the linear model. Let us emphasize that our derivations may be extended to time-varying nominal variables. This alternative approach may be used for instance in sequential linear or quadratic programming for the design of optimal controllers over a fixed time horizon, where the linear time-varying system could be updated after each iteration to consistently drive the iterative solutions closer to the optimal solution. Our approach of linearizing about constant nominal variables is motivated by designing a model-predictive controller that is applied for a moving horizon in which the nominal state and linear dynamics are adaptively updated as time advances.

Equation (16a) is already linear in state, control, and boundary condition variables. Define the  $E \times E$  Jacobian submatrices of the friction term in equation (16b) with respect to  $\boldsymbol{\rho}$  and  $\boldsymbol{\varphi}$ , and subsequently evaluated at the nominal state, by

$$\bar{\alpha} = K \text{diag} \left( \frac{\bar{\boldsymbol{\varphi}} \odot |\bar{\boldsymbol{\varphi}}|}{Q_\ell \bar{\boldsymbol{\rho}}^2} \right), \quad \bar{\beta} = 2K \text{diag} \left( \frac{|\bar{\boldsymbol{\varphi}}|}{Q_\ell \bar{\boldsymbol{\rho}}} \right), \quad (18)$$

respectively, where the square of  $\bar{\boldsymbol{\rho}}$  is evaluated component-wise. Note that the negative sign has been factored out of the  $\bar{\beta}$  term, and the Jacobian submatrices  $\bar{\alpha}$  and  $\bar{\beta}$  are comparable to the coefficients  $\alpha$  and  $\beta$  in equation (3b). Because linearization and the lumped element discretization of the nonlinear PDEs in equation (2) are commutative operations, the set of coefficients  $\alpha$  and  $\beta$  in equation (3b) over each pipe segment in a refined network become the diagonal elements of the matrices  $\bar{\alpha}$  and  $\bar{\beta}$ . The chain rule from vector calculus says that the total derivative of the friction term in equation (16b) with respect to  $\boldsymbol{\rho}$  requires the post-multiplication of  $\bar{\alpha}$  by  $Q_\ell$ .

Linearizing equation (16) in  $\boldsymbol{\rho}$ ,  $\boldsymbol{\varphi}$ ,  $M$ ,  $N$ ,  $\boldsymbol{s}$ , and  $\boldsymbol{w}$  about the nominal state, control, and boundary condition variables and subsequently canceling like terms gives rise to the linear time-invariant system

$$\begin{bmatrix} \dot{\boldsymbol{\rho}} \\ \delta\dot{\boldsymbol{\varphi}} \end{bmatrix} = \bar{A} \begin{bmatrix} \boldsymbol{\rho} \\ \boldsymbol{\varphi} \end{bmatrix} - \begin{bmatrix} \Lambda^{-1} \boldsymbol{w} \\ \sigma^2 L^{-1} (N\bar{\boldsymbol{s}} + M\bar{\boldsymbol{\rho}} + \bar{N}\boldsymbol{s}) \end{bmatrix} + \bar{F}, \quad (19)$$

where the state matrix  $\bar{A}$  and additive nominal term  $\bar{F}$  are given by

$$\bar{A} = \begin{bmatrix} 0 & \Lambda^{-1} Q'X \\ \bar{\alpha} Q_\ell - \sigma^2 L^{-1} \bar{M} & -\bar{\beta} \end{bmatrix} \quad (20)$$

and

$$\bar{F} = \begin{bmatrix} 0 \\ \sigma^2 L^{-1} (\bar{M}\bar{\boldsymbol{\rho}} + \bar{N}\bar{\boldsymbol{s}}) - K \frac{\bar{\boldsymbol{\varphi}} \odot |\bar{\boldsymbol{\varphi}}|}{Q_\ell \bar{\boldsymbol{\rho}}} - \bar{\alpha} Q_\ell \bar{\boldsymbol{\rho}} + \bar{\beta} \bar{\boldsymbol{\varphi}} \end{bmatrix}. \quad (21)$$

The initial condition of the linear system is equal to the initial condition in equation (17). If the nominal variables and linear system dynamics are updated as time

progresses, then the initial condition would likewise be updated to equal the state at the previous time. Let us emphasize that the same symbols have been used to describe the solutions of the nonlinear and linear systems. In the following, we will continue to interchange these symbols when the context is clear. However, if the linear and nonlinear solutions are compared with respect to one another, then they will be clearly distinguished with subscript labels. Before introducing the model-predictive controller, we first analyze the stability of the dynamics (16) and the accuracy of the linear system approximation in the following two sections.

## 6 Eigenvalue and Pole Analysis

Although the pipeline network flows are stable in the control-theoretic sense because physical frictional effects strongly dissipate kinetic energy, analysis of the eigenvalues of the state matrix  $\bar{A}$  is beneficial for the design of controllers and could potentially be used to design a preconditioner for iterative solvers. The closed-form representation of the eigenvalues of the state matrix  $\bar{A}$  has not received much attention and generally does not exist for even the simplest of systems, such as a single discretized pipe. We examine the relationship between the dynamics of gas flow in pipelines and the stability of the governing equations by providing a comprehensive analysis of the eigenvalues of the linearized dynamics matrix  $\bar{A}$ . In addition, relations between the eigenvalues of  $\bar{A}$  and the poles of the transfer matrix from Section 2.2 are discussed.

### 6.1 Eigenvalues of the State Matrix

We begin with the following proposition that establishes an identity on the eigenvalues of the state matrix  $\bar{A}$ .

**Proposition 2** *Let  $\{\zeta(m)\}_{m=1}^{E+V_w}$  be the set of eigenvalues of  $\bar{A}$  in equation (20), where  $E$  and  $V_w$  are the cardinalities of  $\mathcal{E}$  and  $\mathcal{V}_w$ . Then*

$$\sum_{m=1}^{E+V_w} \zeta(m) = - \sum_{k=1}^E \frac{\lambda_k |\bar{\varphi}_k|}{D_k(Q_\ell \bar{\rho})_k}. \quad (22)$$

**Proof** The trace formula for the sum of eigenvalues of  $\bar{A}$  gives the result

$$\sum_{m=1}^{E+V_w} \zeta(m) = - \sum_{k=1}^E \bar{\beta}_{kk} = - \sum_{k=1}^E \frac{\lambda_k |\bar{\varphi}_k|}{D_k(Q_\ell \bar{\rho})_k}.$$

This concludes the proof.  $\square$

We define the *center of gravity* of the eigenvalues of  $\bar{A}$  as the sum  $c = \sum_{m=1}^{E+V_w} \zeta(m) / (E + V_w)$ . Proposition 2 provides a closed-form expression for the center of gravity and shows that it is always negative for physical systems in which densities are always positive, and that it depends on  $\bar{\beta}$  but not on  $\bar{\alpha}$ . The dependency of the center of gravity on  $\bar{\beta}$  is consistent with the initial definition of the frequency domain representation in Section 2.2. A

surprising consequence of Proposition 2 is that the center of gravity does not explicitly depend on the topology of the network described by the incidence sub-matrices  $\bar{M}$  and  $\bar{N}$ . The fact that the center of gravity depends on the properties of each pipeline in the network and not on the topology of the network may suggest that the eigenvalues of the state matrix are approximately equal to the collection of eigenvalues for each individual pipe in the network. We return to this observation later in this section. We first show that the eigenvalues of the state matrix associated with the simplified system described by  $\delta = 0$  and  $\bar{\alpha} = 0$  have strictly negative real parts. Using the results from Section 2, let us suppose that the rates of changes of the boundary conditions are sufficiently small so that this simplified system may be considered.

To simplify the algebra, the actions of the compressors are assumed to be unity in the following theorem. This assumption leads to symmetry of the matrix product  $Q'\bar{M}$  that arises in the state matrix of the simplified system, because the weighted incidence matrix  $\bar{M}$  equals the signed incidence matrix  $Q$  when compressors are bypassed. With  $\delta = 0$  and  $\bar{\alpha} = 0$ , we solve for  $\varphi$  in the lower part of equation (19) and substitute the resulting expression into the upper part of the linear system to obtain the state matrix of the simplified system given by

$$\bar{A} = -\Lambda^{-1}(RQ)'RQ, \quad (23)$$

where  $R$  is the  $E \times E$  diagonal matrix with positive diagonal components  $R_{kk} = \sqrt{\sigma^2 \pi D_k^3 (Q_\ell \bar{\rho})_k / (4\ell_k \lambda_k |\bar{\varphi}|)}$  for  $k \in \mathcal{E}$ . We state a few preliminary results. A real symmetric matrix has strictly positive eigenvalues if and only if it is positive definite [24]. If  $A$  and  $B$  are arbitrary positive definite  $n \times n$  matrices, then  $ABA$  is positive definite [23]. Suppose that  $A$  and  $B$  are positive definite, that  $A$  is diagonal, and consider  $AB = A^{1/2}(A^{1/2}BA^{1/2})A^{-1/2}$ , where  $A^{1/2}$  is the diagonal matrix with diagonal components equal to the square roots of those of  $A$ . Since  $A^{1/2}$  is positive definite, the above result says that  $(A^{1/2}BA^{1/2})$  is positive definite. Therefore,  $AB$  is similar to a positive definite matrix, and must have positive eigenvalues.

**Theorem 1** *Assume that the gas network is connected with no self-loops, and that its compressors are bypassed. Then the  $V_w \times V_w$  state matrix  $\bar{A} = -\Lambda^{-1}(RQ)'RQ$  of the simplified linear system described by  $\delta = 0$  and  $\bar{\alpha} = 0$  has strictly negative real eigenvalues.*

**Proof** As a consequence to Proposition 1, the diagonal matrix  $\Lambda^{-1}$  is positive definite. A result from graph theory states that the number of linearly independent columns of  $\Xi$  for a connected network with  $V$  nodes is  $(V - 1)$  [43]. Because  $Q$  is formed by removing  $V_s \geq 1$  columns from  $\Xi$ , it follows that  $Q$  has full column rank. From Sylvester's rank inequality, the matrix  $RQ$  also has full rank. Thus, the matrix  $(RQ)'RQ$  is invertible and in particular positive definite. The last of the results stated above then shows that  $\Lambda^{-1}(RQ)'RQ$  is similar to a positive definite matrix. Therefore, we conclude that the



eigenvalues of  $\Lambda^{-1}(RQ)'RQ$  are real and positive from which the eigenvalues of  $\bar{A} = -\Lambda^{-1}(RQ)'RQ$  are real and negative.  $\square$

### 6.2 Poles of the Pipeline Transfer Matrix

Although the eigenvalues of the finite-dimensional state matrix  $\bar{A}$  for a single pipe in its refined edge representation and a subset of the infinitely many poles of the irrational transfer matrix  $G(s)$  are generally unequal, the poles have a simple closed formula that can be used to gain insight into the properties of the eigenvalues of  $\bar{A}$ . The poles of each component of  $G(s)$  in equation (6) for  $\alpha = 0$  are given by

$$\zeta^\pm(m) = -\frac{\beta}{2} \pm j \sqrt{\left(\frac{\pi\sigma}{2\ell}\right)^2 (2m+1)^2 - \left(\frac{\beta}{2}\right)^2}, \quad (24)$$

for  $m = 0, 1, \dots$ . Because the scalar  $\beta$  in equation (3b) depends on the nominal density, we may choose the average value of the diagonal components of the matrix  $\bar{\beta}$  and define  $\beta = \sum_{k=1}^E \bar{\beta}_{kk}/E$ . From equation (24), we see that the imaginary asymptote of the poles of  $G(s)$  intersects the real axis of the complex plane at  $s = -\beta/2$ . The following proposition shows that this value is equal to the center of gravity of the eigenvalues of  $\bar{A}$ .

**Proposition 3** *Suppose that  $\beta = \sum_{k=1}^E \bar{\beta}_{kk}/E$ . Then the imaginary asymptote of the poles of  $G(s)$  in equation (6) for a single pipe with one supply node intersects the real axis of the complex plane at the center of gravity of the eigenvalues of  $\bar{A}$  for the discretized pipe.*

**Proof** From Proposition 2, we have the relation  $\beta = -c(E + V_w)/E$ . Because  $E = V_w$  for a single discretized pipe with one supply node, it follows that  $c = -\beta/2$ .  $\square$

The left and right sides of Figure 3(a) depict the poles of  $G(s)$  and the eigenvalues of  $\bar{A}$  for a single pipe. The left and right sides display the effects of two different withdrawal boundary conditions. Figure 3(a) demonstrates the implications of Proposition 3 by confirming that the imaginary asymptote of the poles of  $G(s)$  intersects the real axis of the complex plane at the center of gravity of the eigenvalues of  $\bar{A}$ . The figure also demonstrates that the poles and eigenvalues are qualitatively similar in that few are purely real while many are complex and are collected along the imaginary asymptote. Moreover, the poles of  $G(s)$  provide quantitative approximations to the eigenvalues of  $\bar{A}$  especially for small mass flux boundary condition values. In every case, all of the poles of  $G(s)$  have strictly negative real parts because  $\beta$  in equation (3b) is always positive for nonzero flows. This observation agrees with the asymptotic stability of the system as indicated by Theorem 1.

### 6.3 Poles of the Network Transfer Matrix

In the rest of this section, we distinguish between the edge set  $\mathcal{E}$  of the original network before any refinement and the edge set  $\hat{\mathcal{E}}$  of the refined network. Extending notation from Section 2.2, let us define density

and flow variations  $\mathbf{P}_k(s, x)$  and  $\Phi_k(s, x)$  in the Laplace domain for each edge  $k \in \mathcal{E}$ . These variables are concatenated to form the vectors  $\mathbf{P} = (P_1, \dots, P_E)'$  and  $\Phi = (\Phi_1, \dots, \Phi_E)'$ . Define the matrices  $\alpha = \text{diag}(\alpha_k)$  and  $\beta = \text{diag}(\beta_k)$ , where  $\alpha_k$  and  $\beta_k$  are extended from a single pipe in equation (4) to a network using, as before, nominal density values and steady-state mass flux values for each edge  $k \in \mathcal{E}$ . In general, the matrices  $\alpha$  and  $\beta$  are not the same size nor do they have the same diagonal components as  $\bar{\alpha}$  and  $\bar{\beta}$  in equation (19). The other components of the network transfer matrix are defined by  $\ell = \text{diag}(\ell_k)$ ,  $\gamma(s) = \text{diag}(\gamma_k(s))$ , and  $\mathbf{z}_c(s) = \text{diag}((z_c)_k(s))$ . Following a previous approach [46], the single pipeline transfer matrix representation is extended to the network with the representation

$$\begin{bmatrix} \mathbf{P}^\ell \\ \Phi^0 \end{bmatrix} = \begin{bmatrix} \cosh(\ell\gamma) & -\frac{z_c}{\sigma} \sinh(\ell\gamma) \\ -\sigma z_c^{-1} \sinh(\ell\gamma) & \cosh(\ell\gamma) \end{bmatrix} \begin{bmatrix} \mathbf{P}^0 \\ \Phi^\ell \end{bmatrix}, \quad (25)$$

where for readability we choose the simplified model described by  $\alpha_k = 0$  for all  $k \in \mathcal{E}$ . In the above representation, we use the notation  $g(\ell\gamma) = \text{diag}(g(\ell_k\gamma_k))$  for a complex-valued function  $g$  of a complex argument. For each  $k \in \mathcal{E}$ , the poles appearing in the  $k$ -th and  $(E+k)$ -th rows of the network transfer matrix are given by

$$\zeta_k^\pm(m) = -\frac{\beta_k}{2} \pm j \sqrt{\left(\frac{\pi\sigma}{2\ell_k}\right)^2 (2m+1)^2 - \left(\frac{\beta_k}{2}\right)^2}, \quad (26)$$

for  $m = 0, 1, \dots$ . The form of the above expression for the poles of the network transfer matrix indicates that the complex plane should contain  $E$  imaginary asymptotes about which the eigenvalues of  $\bar{A}$  are collected, where the asymptotes intersect the real axis of the complex plane at  $c_k = -\beta_k/2$  for  $k = 1, \dots, E$ . Proposition 3 indicates that we have  $\beta_k = \sum_{\hat{k} \in \hat{\mathcal{E}}_k} \bar{\beta}_{\hat{k}\hat{k}}/\hat{E}_k$ , where  $\hat{\mathcal{E}}_k \subset \hat{\mathcal{E}}$  denotes the set of edges in the refined network representation of pipe  $k \in \mathcal{E}$  with  $\hat{E}_k$  being the number of elements contained in  $\hat{\mathcal{E}}_k$ . Consider two pipes in a network represented by indices  $k_1, k_2 \in \mathcal{E}$ . The above result implies that the distance  $|c_{k_1} - c_{k_2}|$  between the asymptotes will increase as the difference  $|\beta_{k_1} - \beta_{k_2}|$  between the Jacobian terms increases. A stronger interpretation presents itself if the pipes have the same diameters and friction factors and operate at similar pressures. Indeed, suppose that  $r_{k_1} \approx r_{k_2}$ , where we define *resistance*  $r_k = -\sum_{\hat{k} \in \hat{\mathcal{E}}_k} \lambda_k / (2\hat{E}_k D_k (Q_\ell \bar{\rho})_{\hat{k}})$  for each  $k \in \mathcal{E}$ , in analogy to an electric circuit. Because mass flux in steady-state is uniform along a single pipe, we have

$$c_{k_1} - c_{k_2} = r_{k_1} |\bar{\varphi}_{k_1}| - r_{k_2} |\bar{\varphi}_{k_2}| \approx r_{k_1} (|\bar{\varphi}_{k_1}| - |\bar{\varphi}_{k_2}|).$$

Therefore, in this case, the separation between the two asymptotes will increase as the difference between the mass flux values in the two pipes increases. Moreover, these asymptotes will cross the real axis of the complex plane at approximately the same location if the associated pipelines experience similar mass flux values. Although the values of resistance may not generally agree

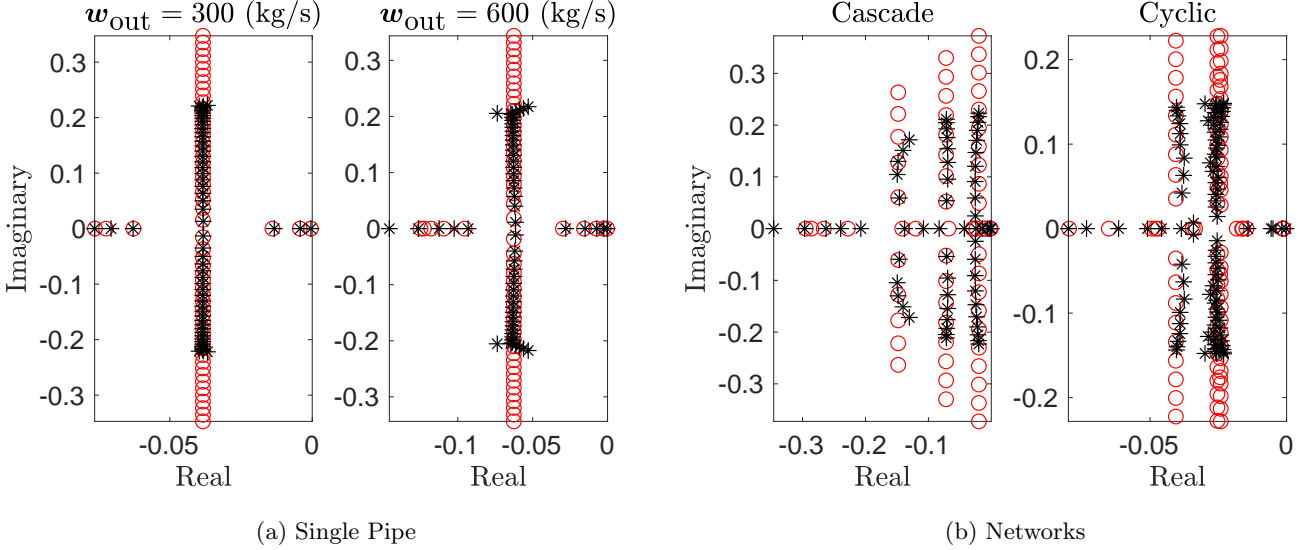


Fig. 3. Eigenvalues (\*) of the unsimplified state matrix  $\bar{A}$  in (20) and poles (o) of the transfer function  $G(s)$  in (6). (a) A single pipe discretized into 30 segments and for two values of mass outflow (left and right). The pipeline parameters are  $\ell = 100$  km,  $D = 0.75$  m,  $\lambda = 0.01$ , and  $\sigma = 377$  m/s. (b) The cascade network (left) consists of a series connection of three pipes with three withdrawal nodes before discretization. The cyclic network (right) is defined below in Figure 4.

throughout a given network, we state this result because it is intuitive for demonstration of the network examples in Figure 3 that we now describe.

First, consider the same pipe in Figure 3(a) with supply at the inlet and withdrawal at the outlet but with two additional withdrawal nodes stationed between the ends of the pipeline at equal intervals. This network is in fact a cascade connection of three pipes of equal length and arises in gunbarrel pipelines [47]. The withdrawal node closest to the supply node experiences outflow of 500 kg/m<sup>2</sup>s, the subsequent node has outflow of 200 kg/m<sup>2</sup>s, and the outlet node has an outflow of 70 kg/m<sup>2</sup>s. From equation (9c), the mass flux of gas in the first pipe is  $\bar{\varphi}_1 = 770$ , that in the second is  $\bar{\varphi}_2 = 270$ , and that in the last pipe is  $\bar{\varphi}_3 = 70$ . Because these mass flux values vary significantly from one another, we expect to see three distinct imaginary asymptotes in the eigenvalues of  $\bar{A}$ . The eigenvalues of  $\bar{A}$  and the poles of the network transfer matrix are shown in the cascade plot on the left side of Figure 3(b). As expected, we observe three imaginary asymptotes in the eigenvalues of  $\bar{A}$ . The right side of Figure 3(b) shows the eigenvalues and poles for the cyclic network displayed in Figure 4 that we further examine below in Section 9. This cyclic network contains five pipes, three of which deliver similar mass flux values, and this is evident in Figure 3(b) by the collection of eigenvalues along three asymptotes parallel to the imaginary axis in the complex plane at approximately  $s = -0.025$ . One imaginary asymptote is clearly isolated and intersects the real axis at approximately  $s = -0.040$ . The fifth imaginary asymptote intersects the real axis at approximately  $s = -0.034$ . This asymptote is not clearly visible likely because the associated pipe contains only one internal discretization node.

## 7 Error Analysis of the Linear Approximation

Throughout the rest of the paper, we generally omit the hat symbols and suppose that  $\mathcal{E}$  denotes the set of edges in the refined graph. In this section, we use Lyapunov theory to examine and quantify the error of the approximate linear dynamics (19) with respect to the nonlinear system (16). The main result is a worst-case bound on the difference between the solutions of the linear and nonlinear systems as a function of time and size of state variation about a nominal state. Specifically, we use  $(\boldsymbol{\rho}, \varphi)$  to denote the solution of the system (16)-(17) and  $(\boldsymbol{\rho}_{\text{lin}}, \varphi_{\text{lin}})$  to denote the solution of the linear approximation (17)-(19) with  $\delta = 1$ , assuming the same initial conditions. For simplicity, we suppose in this section that  $\mathbf{s} = \bar{\mathbf{s}}$ ,  $M = \bar{M}$ , and  $N = \bar{N}$ . This assumption is negligible in practical pipeline operations. The linear system in equation (19) with  $\delta = 1$  becomes

$$\begin{bmatrix} \dot{\boldsymbol{\rho}} \\ \dot{\varphi} \end{bmatrix} = \bar{A} \begin{bmatrix} \boldsymbol{\rho} \\ \varphi \end{bmatrix} + \begin{bmatrix} -\Lambda^{-1} \mathbf{w} \\ -\sigma^2 L^{-1} \bar{N} \bar{\mathbf{s}} - K \frac{\bar{\varphi} \circ |\bar{\varphi}|}{Q_i \bar{\rho}} - \bar{\alpha} Q_i \bar{\boldsymbol{\rho}} + \bar{\beta} \bar{\varphi} \end{bmatrix}. \quad (27)$$

**Theorem 2** Suppose that the real parts of the eigenvalues of  $\bar{A}$  are negative, that  $\mathbf{s} = \bar{\mathbf{s}}$ ,  $M = \bar{M}$ , and  $N = \bar{N}$ , that  $\bar{\varphi}_k > 0$  for all  $k \in \mathcal{E}$ , and that  $\bar{\boldsymbol{\rho}}_j > 0$  for all  $j \in \mathcal{V}_w$ . If, for all  $t \in [0, T)$ , the solution of equation (16) satisfies  $|\boldsymbol{\rho}_j(t) - \bar{\boldsymbol{\rho}}_j| \leq \kappa \bar{\boldsymbol{\rho}}_j$  for all  $j \in \mathcal{V}_w$  and  $|\varphi_k(t) - \bar{\varphi}_k| \leq \kappa \bar{\varphi}_k$  for all  $k \in \mathcal{E}$  with  $\kappa \in [0, \kappa_{\text{max}}]$  and  $\kappa_{\text{max}} < 1$  sufficiently small, then there exist constants  $a, b, c, d > 0$  such that

$$\frac{\|\mathbf{e}(t)\|}{\|(\bar{\boldsymbol{\rho}}, \bar{\varphi})'\|} \leq d \left( \frac{\kappa^2}{(1 - \kappa)^2} a + \frac{\kappa^2}{1 - \kappa} b \right) (1 - e^{-ct}), \quad (28)$$

where  $\mathbf{e} = (\boldsymbol{\rho}, \varphi) - (\boldsymbol{\rho}_{\text{lin}}, \varphi_{\text{lin}})$  and  $\|\mathbf{e}\| = \sqrt{\mathbf{e}'\mathbf{e}}$  is the Euclidean norm of the vector  $\mathbf{e}$ . Note the elapsed time  $T$  could be finite or infinite.

**Proof** Because density and flux are assumed to be positive, the function  $f(\boldsymbol{\rho}, \varphi, \mathbf{w})$  on the right-hand side of equation (16) is continuously differentiable. Invoking the mean value theorem, this function may be written as

$$f = A^* \begin{bmatrix} \boldsymbol{\rho} \\ \varphi \end{bmatrix} + \begin{bmatrix} -\Lambda^{-1} \mathbf{w} \\ -\sigma^2 L^{-1} \bar{N} \bar{\mathbf{s}} - K \frac{\bar{\varphi} \circ |\bar{\varphi}|}{Q_\ell \bar{\boldsymbol{\rho}}} - \alpha^* Q_\ell \bar{\boldsymbol{\rho}} + \beta^* \bar{\varphi} \end{bmatrix}, \quad (29)$$

where

$$A^* = \begin{bmatrix} 0 & \Lambda^{-1} Q' X \\ \alpha^* Q_\ell - \sigma^2 L^{-1} \bar{M} & -\beta^* \end{bmatrix}, \quad (30)$$

$$\alpha^* = K \text{diag} \left( \frac{(\varphi^*)^2}{Q_\ell (\boldsymbol{\rho}^*)^2} \right), \quad \beta^* = 2K \text{diag} \left( \frac{\varphi^*}{Q_\ell \boldsymbol{\rho}^*} \right). \quad (31)$$

Here,  $(\boldsymbol{\rho}^*, \varphi^*)$  is a vector where each entry corresponds to the line segment that connects  $(\boldsymbol{\rho}, \varphi)$  to the nominal state  $(\bar{\boldsymbol{\rho}}, \bar{\varphi})$ . The error vector satisfies

$$\begin{aligned} \dot{\mathbf{e}} &= A^* \begin{bmatrix} \boldsymbol{\rho} \\ \varphi \end{bmatrix} - \bar{A} \begin{bmatrix} \boldsymbol{\rho}_{\text{lin}} \\ \varphi_{\text{lin}} \end{bmatrix} - (A^* - \bar{A}) \begin{bmatrix} \bar{\boldsymbol{\rho}} \\ \bar{\varphi} \end{bmatrix} \\ &= \bar{A} \mathbf{e} + (A^* - \bar{A}) \begin{bmatrix} \boldsymbol{\rho} - \bar{\boldsymbol{\rho}} \\ \varphi - \bar{\varphi} \end{bmatrix}. \end{aligned} \quad (32)$$

The dynamics of  $\mathbf{e}$  contain a linear term and a perturbation term. The difference between the Jacobian matrices in equations (20) and (30) in the latter term reduces to

$$A^* - \bar{A} = \begin{bmatrix} 0 & 0 \\ (\alpha^* - \bar{\alpha}) Q_\ell & -(\beta^* - \bar{\beta}) \end{bmatrix}. \quad (33)$$

The  $k$ -th diagonal entries of the diagonal matrices  $(\alpha^* - \bar{\alpha})$  and  $(\beta^* - \bar{\beta})$  with  $k: i \mapsto j$  are given by

$$\alpha_{kk}^* - \bar{\alpha}_{kk} = K_{kk} \left( \frac{(\varphi_k^*)^2}{(\boldsymbol{\rho}_j^*)^2} - \frac{(\bar{\varphi}_k)^2}{\bar{\boldsymbol{\rho}}_j^2} \right), \quad (34a)$$

$$\beta_{kk}^* - \bar{\beta}_{kk} = 2K_{kk} \left( \frac{\varphi_k^*}{\boldsymbol{\rho}_j^*} - \frac{\bar{\varphi}_k}{\bar{\boldsymbol{\rho}}_j} \right). \quad (34b)$$

Because  $|\boldsymbol{\rho}_j - \bar{\boldsymbol{\rho}}_j| \leq \kappa \bar{\boldsymbol{\rho}}_j$  and  $|\varphi_k - \bar{\varphi}_k| \leq \kappa \bar{\varphi}_k$ , it can be shown that

$$\|\alpha^* - \bar{\alpha}\| \leq \frac{4\kappa}{(1-\kappa)^2} \|\bar{\alpha}\|, \quad \|\beta^* - \bar{\beta}\| \leq \frac{2\kappa}{1-\kappa} \|\bar{\beta}\|, \quad (35)$$

where the matrix norm is defined as the induced Euclidean norm. The perturbation term on the right-hand side of equation (32) is therefore bounded according to

$$\begin{aligned} &\|(A^* - \bar{A})(\boldsymbol{\rho} - \bar{\boldsymbol{\rho}}, \varphi - \bar{\varphi})'\| \\ &\leq (\|\alpha^* - \bar{\alpha}\| \|Q_\ell\| + \|\beta^* - \bar{\beta}\|) \|\kappa(\bar{\boldsymbol{\rho}}, \bar{\varphi})'\| \\ &\leq \left( \frac{\kappa^2}{(1-\kappa)^2} a + \frac{\kappa^2}{1-\kappa} b \right) \|(\bar{\boldsymbol{\rho}}, \bar{\varphi})'\|, \end{aligned} \quad (36)$$

where  $a = 4\|\bar{\alpha}\| \|Q_\ell\|$  and  $b = 2\|\bar{\beta}\|$ .

The remaining part of the proof uses standard Lyapunov stability analysis arguments [24]. Because the

eigenvalues of  $\bar{A}$  are assumed to have negative real parts, there exists a Lyapunov function of the form  $V(\mathbf{e}(t)) = \mathbf{e}'(t)W\mathbf{e}(t)$ , where  $W$  is a symmetric positive definite matrix that satisfies the Lyapunov equation  $\bar{A}'W + W\bar{A} = -I$ , with  $I$  being the identity matrix. The time dependence of  $\mathbf{e}$  will be suppressed for readability. The time derivative of  $V(\mathbf{e})$  along the trajectories of the error dynamics in equation (32) is bounded by

$$\dot{V}(\mathbf{e}) \leq -\|\mathbf{e}\|^2 + \Gamma\|\mathbf{e}\|, \quad (37)$$

where

$$\Gamma = 2\|W\| \left( \frac{\kappa^2}{(1-\kappa)^2} a + \frac{\kappa^2}{1-\kappa} b \right) \|(\bar{\boldsymbol{\rho}}, \bar{\varphi})'\|. \quad (38)$$

Next, define  $Z(\mathbf{e}) = \sqrt{V(\mathbf{e})}$ . Because  $W$  is symmetric, it has real eigenvalues. It follows from Rayleigh's quotient that  $\lambda_1 \|\mathbf{e}\|^2 \leq V(\mathbf{e}) \leq \lambda_2 \|\mathbf{e}\|^2$ , where  $\lambda_1$  and  $\lambda_2$  are the minimum and maximum eigenvalues of  $W$ . For  $V(\mathbf{e}) > 0$ ,  $\dot{Z}(\mathbf{e}) \leq (-Z(\mathbf{e})/2\lambda_2 + \Gamma/2\sqrt{\lambda_1})$ . Therefore, from the comparison lemma, we have

$$\begin{aligned} Z(t) &\leq \frac{\Gamma}{2\sqrt{\lambda_1}} \int_0^t e^{-(t-\tau)/2\lambda_2} d\tau \\ &= \frac{\lambda_2 \Gamma}{\sqrt{\lambda_1}} \left( 1 - e^{-t/2\lambda_2} \right) \leq \frac{\lambda_2 \Gamma}{\sqrt{\lambda_1}}. \end{aligned} \quad (39)$$

Finally, it can be shown that the above inequality also holds for  $V = 0$  [24]. The proof is completed by rearranging Rayleigh's quotient into the form

$$\|\mathbf{e}\| \leq \sqrt{\frac{V}{\lambda_1}} = \frac{Z}{\sqrt{\lambda_1}} \leq \frac{\lambda_2}{\lambda_1} \Gamma \left( 1 - e^{-t/2\lambda_2} \right), \quad (40)$$

with  $c = 1/(2\lambda_2)$  and  $d = 2\|W\| \lambda_2/\lambda_1$ .  $\square$

In the proof of Theorem 2, we assume that  $\kappa \leq \kappa_{\max}$  to ensure that the nonlinear solution is well-defined. Calibration of maximal appropriate values of  $\kappa_{\max}$  depends on empirical observations and is beyond our scope.

The bound on the right-hand side of equation (28) is called the *error bound* and is denoted by

$$\mathbf{E}(t; \kappa) = d \left( \frac{\kappa^2}{(1-\kappa)^2} a + \frac{\kappa^2}{1-\kappa} b \right) (1 - e^{-ct}). \quad (41)$$

The coefficients  $a$ ,  $b$ ,  $c$ , and  $d$  depend on the the nominal state and the parameters of the network. Observe that  $\mathbf{E}(0; \kappa) = 0$  and that  $\mathbf{E}(t; \kappa)$  monotonically increases and converges to a finite upper bound for each  $\kappa \leq \kappa_{\max}$  as  $t$  increases without bound. From Taylor's theorem, the error bound in equation (41) is in fact approximately linear over a sufficiently small time window of operation for each value of  $\kappa \leq \kappa_{\max}$ . The slope of the best fit line over a 60 second time window is documented in Table 1 for several values of  $\kappa$ . Because the boundary conditions are expected to vary slowly over a span of hours and not seconds, we consider the small values of  $\kappa$  in Table 1 to be reasonable. The tabulated slopes indicate that if  $t$  and  $\kappa$  are sufficiently small, then the error bound will be

Table 1

Initial slope of the error bound in equation (41) over  $t \in [0, 60]$  (s) for various values of  $\kappa$  using the network topology and parameters from Fig. 4.

$\kappa$	0.2%	0.4%	0.6%	0.8%	1.0%
$\text{slope}\{E(t; \kappa)\}$	0.003	0.011	0.025	0.045	0.07

small as well and the worst-case estimate is analytically quantified by  $E(t; \kappa)$ .

Although the error bound is derived conservatively without regard to the rates of changes in the flow variables, it is nonetheless appealing and may have practical implications. The error bound provides a baseline to determine necessary frequencies of a feedback controller with which the linear system dynamics (19) may adequately approximate the nonlinear dynamics (16). As an illustration, suppose that operators of a pipeline network of the form described in Figure 4 can tolerate  $E(t; \kappa) \leq 1$  for 0.6% variations about the nominal state. Table 1 suggests that the operators should be prepared to update the nominal state and linear system approximately every  $1/0.025 = 40$  seconds for the linear system to retain the tolerated error bound. This is considered to be practical for some pipeline systems. For example, meter stations at custody transfer locations usually sample data at least every few seconds in order to appropriately account for the value of the transferred gas. We conclude that if measurements are collected with sufficient frequency such that the nominal state estimate, predicted boundary conditions, and approximate linear evolution dynamics can be updated every 40 seconds, then operators of this network would be assured that the linear solution will remain accurate to within the tolerated error (up to uncertainty in the nonlinear model parameters). This example inspires a model-predictive control design for compressor management in which initial conditions and dynamics are adaptively updated as the time window advances.

## 8 Model-Predictive and Optimal Control

Following applications in gas reservoir storage [21] and coordinated scheduling with electric power systems [51], we seek time-dependent compressor operating schedules that guarantee that limits on pipeline pressures are satisfied as withdrawals by customers are made, and while minimizing energy used for compression [3, 49]. We design a moving-horizon model-predictive controller (MH-MPC) that recursively achieves these conditions by optimizing flows locally in time and utilizing feedback with a moving time window to complete the operation over the entire predictive interval. The frequency of feedback measurements of the MPC is defined by the user. This results in a sampling of the entire time interval  $[0, T]$  at discrete times  $t_m$  evenly spaced by  $\Delta t = t_m - t_{m-1}$ . To compare the outcomes of using the nonlinear system and the adaptive linear system as dynamic constraints, we introduce two model-predictive controllers. One of the controllers uses the nonlinear system (16) as its dynamic

constraints and the other uses the linear approximation (19). For comparison, we also synthesize a single-horizon optimal controller (SHOC) that performs a single optimization to minimize compressor energy over the entire time interval  $[0, T]$ . In the following, we assume a zero-order hold framework in which the compressor actions are constant between sampling times.

### 8.1 Moving-Horizon Model-Predictive Control

At the local time window  $(t_{m-1}, t_m]$ , we are in search of a minimizer of the cost objective function defined by [45, 49]

$$\mathcal{J}(t_m) = \sum_{k \in \mathcal{C}} c_k \varphi_k(t_m) \left( \mu_k(t_m)^{(\gamma-1)/\gamma} - 1 \right), \quad (42)$$

where  $c_k$  is related to the efficiency of the compressor  $k \in \mathcal{C}$  and  $\gamma$  is the isentropic exponent of natural gas [29]. Correspondingly, we also consider the linearized energy expenditure defined by

$$\begin{aligned} \mathcal{J}(t_m) = & \sum_{k \in \mathcal{C}} c_k \varphi_k(t_m) \left( \bar{\mu}_k^{(\gamma-1)/\gamma} - 1 \right) \\ & + \sum_{k \in \mathcal{C}} c_k \left( \frac{\gamma-1}{\gamma} \bar{\varphi}_k \bar{\mu}_k^{-1/\gamma} \right) \mu_k(t_m). \end{aligned} \quad (43)$$

Gas pipeline operations require line pressures and compressor settings to remain within engineering limits. These restrictions are enforced for both controllers using inequality constraints of the form

$$\boldsymbol{\rho}^{\min} \leq \boldsymbol{\rho}(t_m) \leq \boldsymbol{\rho}^{\max}, \quad 1 \leq \mu_k(t_m) \leq \mu_k^{\max}, \quad (44)$$

where  $\boldsymbol{\rho}^{\min}$ ,  $\boldsymbol{\rho}^{\max}$ , and  $\mu_k^{\max}$  are specified bounds. In addition to these inequality constraints, by implicitly integrating the continuous dynamics over the time interval  $(t_{m-1}, t_m]$  the local dynamic constraints are defined by

$$\begin{bmatrix} \boldsymbol{\rho}(t_m) \\ \varphi(t_m) \end{bmatrix} = \begin{bmatrix} \bar{\boldsymbol{\rho}} \\ \bar{\varphi} \end{bmatrix} + \Delta t \bar{f}(\boldsymbol{\rho}(t_m), \varphi(t_m), \mu_k(t_m)), \quad (45)$$

where  $\bar{f}$  represents the right-hand side of either the nonlinear system (16) or the updated linear system (19).

The solution  $\boldsymbol{\rho}^*(t)$ ,  $\varphi^*(t)$ , and  $\mu_k^*(t)$  for  $k \in \mathcal{C}$  at time  $t = t_m$  is determined by solving the optimization problem

$$\text{minimize} \quad \text{Compressor energy: (42) or (43),} \quad (46a)$$

$$\text{subject to} \quad \text{Inequality constraint: (44),} \quad (46b)$$

$$\text{Dynamic constraint: (45).} \quad (46c)$$

The solution to problem (46) is used to update the nominal variables  $\bar{\boldsymbol{\rho}} = \boldsymbol{\rho}^*(t_m)$ ,  $\bar{\varphi} = \varphi^*(t_m)$ , and  $\bar{\mu}_k = \mu_k^*(t_m)$ . By updating the adaptive linear system to realize the current dynamics, the process is thereafter repeated for the subsequent time interval  $(t_m, t_{m+1}]$ . The MPC is initiated by defining the nominal state to be the initial condition in equation (17).

## 8.2 Single-Horizon Optimal Control

As discussed in the introduction, a common approach to design compressor operating protocols is to minimize the energy expended over the entire predictive horizon  $[0, T]$  subject to dynamic constraints and anticipated loads [49]. The objective function for such single-horizon optimal control (SHOC) is defined by

$$J = \sum_{m=1}^{\nu} \mathcal{J}(t_m), \quad (47)$$

where  $\mathcal{J}(t_m)$  is given by one of equations (42) or (43) depending on whether nonlinear or linear programs are considered. As with MH-MPC, the linear and nonlinear programs for the SHOC design are both implemented in order to compare the use of linear or nonlinear representations as the dynamic constraints. The SHOC dynamic constraints are defined to be the collection of equations (45) for all  $m = 1, \dots, \nu$ , which are derived using either a fixed linear system (19) or the nonlinear system (16).

The SHOC approach accounts for variations in boundary conditions anticipated to occur throughout the entire time horizon  $[0, T]$ , and provides a least cost policy for the actions of the compressors prior to performing the operation. In contrast, the proposed MH-MPC only accounts for the current state and the predicted boundary conditions in the next immediate time step. Consequently, we expect the solution obtained using MH-MPC to be sub-optimal in terms of expended energy. However, the sequence of MH-MPC solves requires less computational time than the single SHOC solve, which is significant for larger networks. Implementing MH-MPC could therefore enable operations that are more responsive to unanticipated changes in loads. We illustrate these solution techniques for two linear programming problems. Although more efficient algorithms may exist, a proposed method for linear programming with efficient matrix multiplication algorithms and low rank incremental updating of inverses has a worst-case computational time performance on the order of  $\mathcal{O}(\nu^{2.5}(E + V_w)^{2.5})$  for SHOC [44], and the corresponding performance is  $\mathcal{O}(\nu(E + V_w)^{2.5})$  for MH-MPC. This suggests that MH-MPC requires a computational time that is smaller than that required by SHOC by a factor of  $\nu^{1.5}$  in the worst-case scenario. For example, 1-hr sampling of a 24-hr horizon gives  $\nu^{1.5} = 125$ .

## 9 Computational Examples

Two examples are showcased to compare the performances of the various control designs. To validate MH-MPC in comparison to SHOC, we consider computational run time and accumulated compressor energy over the entire window of operation as defined in equation (47). To validate the adaptive linear system in comparison to a fixed linear system, we analyze the absolute maximum relative error in the state and control variables between the solutions of the linear and nonlinear

programs for both MH-MPC and SHOC. The error metric for the density variable is defined by

$$e_{\rho} = 2 \max_{j,m} \left| \frac{(\rho_{\text{non}})_j(t_m) - (\rho_{\text{lin}})_j(t_m)}{(\rho_{\text{non}})_j(t_m) + (\rho_{\text{lin}})_j(t_m)} \right|, \quad (48)$$

in which absolute values and division of vectors are applied componentwise. Similar definitions are made for errors in mass flux and compressor control values and are denoted by  $e_{\varphi}$  and  $e_{\mu}$ , respectively. The simulations of these control methods are implemented in Matlab R2023a with sequential quadratic programming using the general-purpose solver `fmincon`. Computations are performed on a MacBook Pro with 32 GB of usable memory. Solutions of the linear programs are computed and subsequently used to initialize the nonlinear programs for both controllers.

### 9.1 5-Node Cyclic Network

Our first network example has the topology depicted in Figure 4 and was used in previous studies to validate a staggered grid discretization method [20]. The blue node is the only supply node at which the boundary condition  $\mathbf{s}_{\text{blue}} = 21 \text{ kg/m}^3$  is specified. The boundary conditions for loads at withdrawal nodes are depicted in Figure 4. We use  $\rho^{\text{min}} = 21 \text{ kg/m}^3$ ,  $\rho^{\text{max}} = 35 \text{ kg/m}^3$ , and  $\mu_k^{\text{max}} = 1.7$  for all  $k \in \mathcal{C}$  as the lower and upper bounds in equation (44). The five edges of this network are discretized into 48 refined segments with  $\ell_k = 5 \text{ km}$  for all  $k \in \mathcal{E}$ . The size of the state matrix  $\bar{A}$  is  $95 \times 95$  and there are three compressor stations for which the control policies will be designed to minimize energy expenditure. The time interval  $[0, T]$  with  $T = 24 \text{ hr}$  is discretized into 24 subintervals using 25 evenly-spaced sampling times. Thus, the linear and nonlinear internal programs of the MH-MPC contain 98 decision variables at each time step. The linear and nonlinear programs corresponding to SHOC contain  $25 \times 98 = 2450$  decision variables each.

Observe in Figure 4 that MH-MPC and SHOC both determine appropriate control actions in the sense that bounds on compression and system pressures are maintained and flow dynamics are adequately represented. Although the solutions of MH-MPC and SHOC are qualitatively similar, there are some differences. MH-MPC leads to greater mass flux at the downstream nodes in all pipes in comparison to optimal control. Additionally, the energy used for control actions arising from MH-MPC is more equally distributed than among the three compressors than in the SHOC solution, in which the red compressor operates at its limits over an extended period of time. Examining Table 2, we see that the cumulative energy used in MH-MPC is nearly identical to that of SHOC for this example. Moreover, the computational run time for SHOC is approximately 20 times larger than that for MH-MPC. As expected from Theorem 2, the relative errors between the linear and nonlinear state variables are smaller when computed with MH-MPC using adaptive linear systems than with SHOC using a fixed linear system.

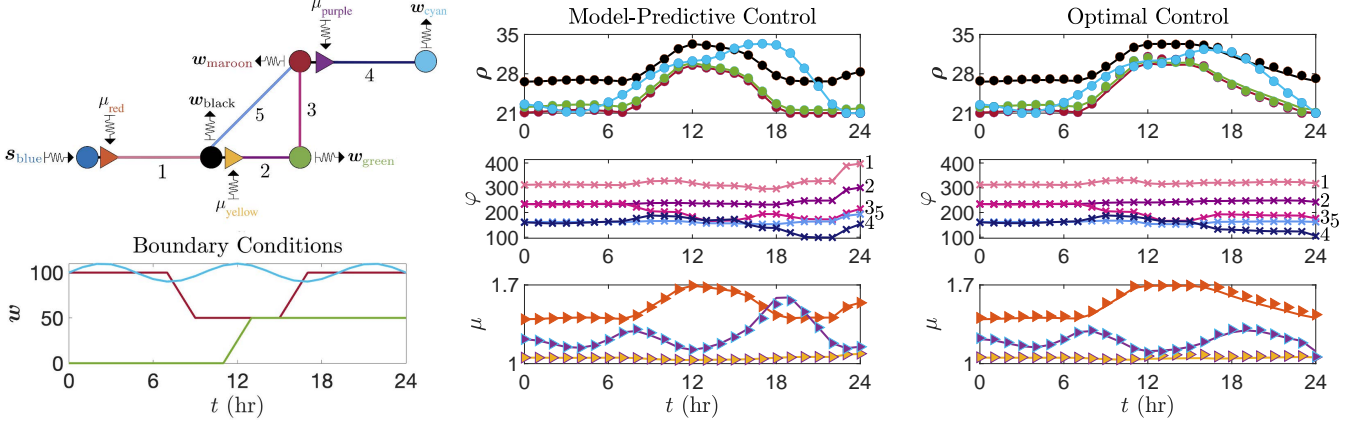


Fig. 4. Left: Network configuration (not to scale) and boundary conditions at color-coordinated nodes. Lines, circles, and triangles in the network diagram represent pipelines, nodes, and compressors, respectively. Pipe lengths in km are  $\ell_1 = 20$ ,  $\ell_2 = 70$ ,  $\ell_3 = 10$ ,  $\ell_4 = 80$ ,  $\ell_5 = 60$ . The pipes have diameter  $D_k = 0.9144$  m and friction factor  $\lambda_k = 0.01$  for  $k = 1, 2, 3$ , and 4, except for edge  $5 \in \mathcal{E}$  for which  $D_5 = 0.635$  m and  $\lambda_5 = 0.015$ . The sound speed is  $\sigma = 377.964$  m/s. Center: moving-horizon model-predictive control (MH-MPC). Right: single-horizon optimal control (SHOC). Solid lines and markers represent solutions obtained using nonlinear and linear dynamics, respectively. The colors of density, flux, and compressor ratio plots correspond to respective locations in the network.

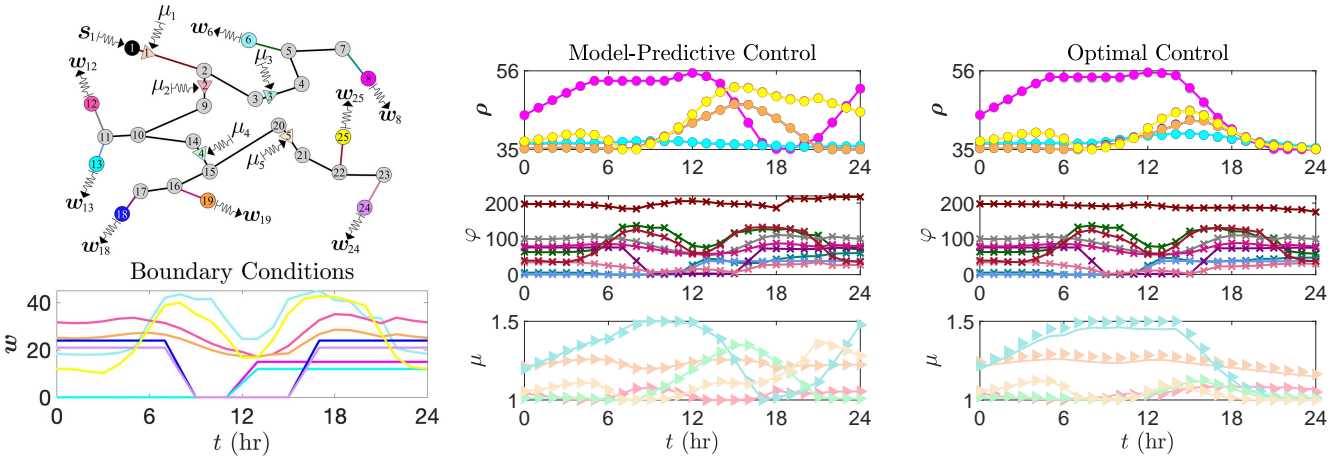


Fig. 5. Left: Network diagram (not to scale) and boundary conditions at color-coordinated nodes [48]. Center: MH-MPC; and Right: SHOC. The sound speed is  $\sigma = 377.964$  m/s, the total pipe length is 477 km, the friction factor is  $\lambda_k = 0.01$  for all  $k \in \mathcal{E}$ , and the diameters vary between 0.6096 m and 0.9144 m.

Table 2  
Computational results of MH-MPC and SHOC for the 5-node cyclic network in Figure 4.

	Run Time	$J$	$e_\rho$	$e_\varphi$	$e_\mu$
MH-MPC	6 s	979.5	0.4%	0.7%	4.6%
SHOC	125 s	978.9	4.0%	1.3%	4.4%

Table 3  
Computational results of MH-MPC and SHOC for the 25-node tree network in Figure 5.

	Run Time	$J$	$e_\rho$	$e_\varphi$	$e_\mu$
MH-MPC	4 s	419.3	0.3%	1.3%	1.9%
SHOC	244 s	341.2	2.8%	1.2%	3.5%

## 9.2 25-Node Tree Network

Our second example uses the 25-node tree network with 5 compressors shown in Figure 5. This network was examined in previous studies to demonstrate a similar SHOC method to the one developed here [49]. Node 1 is the only supply node at which the boundary condition  $s_1 = 35$  kg/m<sup>3</sup> is specified. We use  $\rho^{\min} = 35$  kg/m<sup>3</sup>,  $\rho^{\max} = 56$  kg/m<sup>3</sup>, and  $\mu_k^{\max} = 1.5$  for all  $k \in \mathcal{C}$  in equation (44). The 24 edges of the network are discretized into refined segments in such a way that  $\ell_k \leq 10$  km for all  $k \in \mathcal{E}$ . The size of the state matrix  $\bar{A}$  is  $137 \times 137$  and there are five compressor stations. The time interval  $[0, T]$  with  $T = 24$  hr is discretized into 25 evenly-spaced sampling times. In this case, the linear and nonlinear internal programs of the MH-MPC contain 142 decision variables at each time step. The linear and non-

linear programs corresponding to SHOC each contain  $25 \times 142 = 3550$  decision variables.

The results of MH-MPC and SHOC are displayed in Figure 5. As with the 5-node network example, the solutions computed with the two controllers exhibit similar qualitative behavior among one another. In fact, specific properties observed for the 5-node network can be seen for the 25-node network. First, mass flux increases at the end of the time horizon at least in the supplying pipeline. Second, as in the 5-node example, MH-MPC leads compressor actions to be distributed more evenly among the five compressors than SHOC. Third, the SHOC solution causes compressors to operate at full capacity for longer than those computed with MH-MPC. We conclude this example by examining Table 3. First, in contrast to the 5-node example, observe that the control actions of the 25-node example appear to expend considerably more energy when computed with MH-MPC than with SHOC. Second, although the optimization problems for the 25-node example contain greater numbers of decision variables than the respective problems for the 5-node example, the computation run time for MH-MPC decreased by 2 seconds in going from the 5-node to the 25-node network whereas the SHOC increased by 119 seconds. Also in contrast to the 5-node example, the relative maximum error in flux computed with MH-MPC in the current example is greater than that computed with SHOC.

## 10 Conclusions

This paper presents a comprehensive analysis of adaptive linear system approximations applied to the development of control systems for predictive natural gas pipeline operations. We examine Laplace transform and transfer matrix methods for computationally efficient approximation of the governing pipeline flow equations to quantify the response to variations in boundary conditions. Following a network flow formulation, a lumped element discretization method is applied in space to derive a nonlinear control system of ODEs. An adaptive linear control system is derived to govern local flow dynamics about an arbitrary nominal state. This scalable formulation of a linear control system enables rapid updating of the nominal state and linear system parameters for use in a moving-horizon model-predictive controller (MH-MPC) in which the dynamic constraints are ensured to remain applicable as time progresses and boundary conditions vary. Asymptotic stability properties of the linear system and transfer matrix are then examined. The eigenvalues of the state matrix are proven to have negative real parts and an expression for the center of gravity is derived. The center of gravity of the eigenvalues of the state matrix is shown to be located at exactly where the imaginary asymptote of the poles of the transfer matrix intersects the real axis of the complex plane. The eigenvalue and pole analysis of a single pipe is extended to a network to provide approximate analytical expressions for the eigenvalues of the state matrix. Furthermore, a rigorous bound on the error between the solutions of the

linear and nonlinear systems is derived for general network topologies using Lyapunov theory. The bound depends on the elapsed time and the variation about the nominal state. Assuming that flow and pressure meters collect data with sufficient frequency, the error bound may provide a practical tool in the planning process of operations to check whether the solution of the linear system may be accurate to within an analytically quantifiable tolerance.

In addition to the analysis of linear systems, we develop controllers that seek to minimize the energy expended by compressors in controlling transient pipeline flows. The quantifiable error bound and adaptive linear control system motivate the development of a moving-horizon model-predictive controller to reduce computational run time for the predictive design of transient compressor controls. MH-MPC is formulated subject to nonlinear and adaptive linear system constraints to analyze the resulting error and compare it to the bound derived using Lyapunov theory. Moreover, an optimal controller defined over the entire time horizon is presented so that the results of MH-MPC can be compared to those of the baseline optimal solution. The various controllers are demonstrated on two test network examples. The results showcase that MH-MPC is well-equipped to adapt in local time to changes in system parameters and boundary conditions and may have the potential to significantly reduce the computational time in comparison to the optimal solution. However, the results also demonstrate that a trade-off can occur between computational time and energy used by compressors when comparing MH-MPC to SHOC solutions. Pipeline operators could perform comparisons between the two types of controllers using operational data to further characterize any trade-off for their expected operations. Such examinations could lead to decision support methods that enable more responsive operations that maintain reliability.

## Acknowledgements

The authors are very grateful to Cody W. Allen and Saif R. Kazi for numerous helpful discussions and to E. Olga Skowronek for additional discussions and drawing the network diagrams in Figures 2, 4, and 5. This study was supported by the U.S. Department of Energy’s Advanced Grid Modeling (AGM) project “Dynamical Modeling, Estimation, and Optimal Control of Electrical Grid-Natural Gas Transmission Systems,” the U.S. Department of Energy through the LANL/LDRD Program, and the Center for Non-Linear Studies. Research conducted at Los Alamos National Laboratory is done under the auspices of the National Nuclear Security Administration of the U.S. Department of Energy under Contract No. 89233218CNA000001. L. Baker would like to thank Arizona State University for additional support. S. Shivakumar was supported by the National Science Foundation grants No. 1739990 and 1935453. Report number: LA-UR-23-24798.

## References

- [1] Hans Aalto. Real-time optimisation of natural gas pipeline systems—a simplified approach. *IFAC Proceedings Volumes*, 39(14):167–172, 2006.
- [2] Hans Aalto. Model predictive control of natural gas pipeline systems—a case for constrained system identification. *IFAC-PapersOnLine*, 48(30):197–202, 2015.
- [3] Mohammad Abbaspour and Kirby S. Chapman. Nonisothermal Transient Flow in Natural Gas Pipeline. *Journal of Applied Mechanics*, 75(3), 2008.
- [4] Rezvan Alamian, Morteza Behbahani-Nejad, and Afshin Ghanbarzadeh. A state space model for transient flow simulation in natural gas pipelines. *Journal of Natural Gas Science and Engineering*, 9:51–59, 2012.
- [5] Cody Allen, Roman Zamotorin, Avneet Singh, and Rainer Kurz. Gas pipeline transient modeling via transfer functions: Field data validations. In *PSIG Annual Meeting*, pages PSIG–2205. PSIG, 2022.
- [6] Luke Baker, Dieter Armbruster, Anna Scaglione, and Rodrigo B. Platte. Analysis of a model of a natural gas pipeline—a transfer function approach. *Transactions of Mathematics and Its Applications*, 5(1):tnab002, 2021.
- [7] Luke S Baker. *Gas Mixture Dynamics in Pipeline Networks with a Focus on Linearization and Optimal Control*. PhD thesis, Arizona State University, 2023.
- [8] Luke S. Baker, Saif R. Kazi, Rodrigo B. Platte, and Anatoly Zlotnik. Optimal control of transient flows in pipeline networks with heterogeneous mixtures of hydrogen and natural gas. In *2023 American Control Conference (ACC)*, pages 1221–1228, 2023.
- [9] Morteza Behbahani-Nejad and Younes Shekari. The accuracy and efficiency of a reduced-order model for transient flow analysis in gas pipelines. *Journal of Petroleum Science and Engineering*, 73(1-2):13–19, 2010.
- [10] Aleksandr Beylin, Aleksandr M Rudkevich, and Anatoly Zlotnik. Fast transient optimization of gas pipelines by analytic transformation to linear programs. In *PSIG annual meeting*, pages PSIG–2003. OnePetro, 2020.
- [11] Daniel De Wolf and Yves Smeers. The gas transmission problem solved by an extension of the simplex algorithm. *Management Science*, 46(11):1454–1465, 2000.
- [12] Pia Domschke, Bjorn Geißler, Oliver Kolb, Jens Lang, Alexander Martin, and Antonio Morsi. Combination of nonlinear and linear optimization of transient gas networks. *INFORMS Journal on Computing*, 23(4):605–617, 2011.
- [13] Klaus Ehrhardt and Marc C. Steinbach. Nonlinear optimization in gas networks. In *Modeling, simulation and optimization of complex processes*, pages 139–148. Springer, 2005.
- [14] Michael Bos Feldman. Optimization of gas transmission systems using linear programming. In *PSIG Annual Meeting*, pages PSIG–8809. PSIG, 1988.
- [15] Ajit Gopalakrishnan and Lorenz T Biegler. Economic nonlinear model predictive control for periodic optimal operation of gas pipeline networks. *Computers & Chemical Engineering*, 52:90–99, 2013.
- [16] Sara Grundel, Nils Hornung, Bernhard Klaassen, Peter Benner, and Tanja Cleeß. Computing surrogates for gas network simulation using model order reduction. In *Surrogate-Based Modeling and Optimization*, pages 189–212. Springer, 2013.
- [17] Martin Gugat, Falk M Hante, and Li Jin. Closed loop control of gas flow in a pipe: stability for a transient model. *at-Automatisierungstechnik*, 68(12):1001–1010, 2020.
- [18] Martin Gugat, Michael Herty, Axel Klar, Günter Leugering, and Veronika Schleper. Well-posedness of networked hyperbolic systems of balance laws. *Constrained Optimization and Optimal Control for Partial Differential Equations*, 160:123–146, 2012.
- [19] Martin Gugat and Stefan Ulbrich. The isothermal euler equations for ideal gas with source term: Product solutions, flow reversal and no blow up. *Journal of Mathematical Analysis and Applications*, 454(1):439–452, 2017.
- [20] Vitaliy Gyrya and Anatoly Zlotnik. An explicit staggered-grid method for numerical simulation of large-scale natural gas pipeline networks. *Applied Mathematical Modelling*, 65:34–51, 2019.
- [21] Sai Krishna K. Hari, Kaarthik Sundar, Shriram Srinivasan, Anatoly Zlotnik, and Russell Bent. Operation of natural gas pipeline networks with storage under transient flow conditions. *IEEE Transactions on Control Systems Technology*, 30(2):667–679, 2021.
- [22] Christian Himpe, Sara Grundel, and Peter Benner. Model order reduction for gas and energy networks. *Journal of Mathematics in Industry*, 11(1):1–46, 2021.
- [23] Roger A. Horn and Charles R. Johnson. *Matrix Analysis*. Cambridge University Press, 2012.
- [24] Hassan K. Khalil. *Nonlinear Systems*. Pearson Education. Prentice Hall, 2002.
- [25] Jaroslav Králik, Petr Stiegler, Zdeněk Vostrý, and Jiří Závorka. Modeling the dynamics of flow in gas pipelines. *IEEE Transactions on Systems, Man, and Cybernetics*, (4):586–596, 1984.
- [26] Jaroslav Králik, Petr Stiegler, Zdeněk Vostrý, and Jiří Závorka. A universal dynamic simulation model of gas pipeline networks. *IEEE Transactions on Systems, Man, and Cybernetics*, (4):597–606, 1984.
- [27] Cong Liu, Mohammad Shahidehpour, and Jianhui Wang. Coordinated scheduling of electricity and natural gas infrastructures with a transient model for natural gas flow. *Chaos: An Interdisciplinary Journal of Nonlinear Science*, 21(2):025102, 2011.
- [28] Cesar A. Luongo. An efficient program for transient



- flow simulation in natural gas pipelines. In *PSIG Annual Meeting*, pages PSIG-8605. OnePetro, 1986.
- [29] Ivan Marić, Antun Galovic, and Tomislav Smuc. Calculation of natural gas isentropic exponent. *Flow Measurement and Instrumentation*, 16:13–20, 03 2005.
- [30] Dardo Marqués and Manfred Morari. On-line optimization of gas pipeline networks. *Automatica*, 24(4):455–469, 1988.
- [31] Sidhant Misra, Michael W. Fisher, Scott Backhaus, Russell Bent, Michael Chertkov, and Feng Pan. Optimal compression in natural gas networks: A geometric programming approach. *Transactions on Control of Network Systems*, 2(1):47–56, 2014.
- [32] Andrzej Osiadacz. Simulation of transient gas flows in networks. *International Journal for Numerical Methods in Fluids*, 4(1):13–24, 1984.
- [33] Andrzej J. Osiadacz and Maciej Chaczykowski. Comparison of isothermal and non-isothermal pipeline gas flow models. *Chemical Engineering Journal*, 81(1-3):41–51, 2001.
- [34] Peter B. Percell and Michael J. Ryan. Steady state optimization of gas pipeline network operation. In *PSIG annual meeting*, pages PSIG-8703. OnePetro, 1987.
- [35] Henry H. Rachford Jr. and Richard G. Carter. Optimizing pipeline control in transient gas flow. In *PSIG annual meeting*, pages PSIG-0004. PSIG, 2000.
- [36] H. Prashanth Reddy, Shankar Narasimhan, and S. Murty Bhallamudi. Simulation and state estimation of transient flow in gas pipeline networks using a transfer function model. *Industrial & Engineering Chemistry Research*, 45(11):3853–3863, 2006.
- [37] H. Prashanth Reddy, Shankar Narasimhan, S. Murty Bhallamudi, and S. Bairagi. Leak detection in gas pipeline networks using an efficient state estimator. part-i: Theory and simulations. *Computers & Chemical Engineering*, 35(4):651–661, 2011.
- [38] Justin Ruths, Anatoly Zlotnik, and Shin Li. Convergence of a pseudospectral method for optimal control of complex dynamical systems. In *50th Conference on Decision and Control*, pages 5553–5558. IEEE, 2011.
- [39] Shriram Srinivasan, Kaarthik Sundar, Vitaliy Gyrya, and Anatoly Zlotnik. Numerical solution of the steady-state network flow equations for a non-ideal gas. *IEEE Transactions on Control of Network Systems*, 2022.
- [40] Marc C Steinbach. On pde solution in transient optimization of gas networks. *Journal of computational and applied mathematics*, 203(2):345–361, 2007.
- [41] Kaarthik Sundar and Anatoly Zlotnik. State and parameter estimation for natural gas pipeline networks using transient state data. *IEEE Transactions on Control Systems Technology*, 27(5):2110–2124, 2018.
- [42] A. R. D. Thorley and C. H. Tiley. Unsteady and transient flow of compressible fluids in pipelines—a review of theoretical and some experimental studies. *International journal of heat and fluid flow*, 8(1):3–15, 1987.
- [43] Krishnaiyan Thulasiraman and Madisetti N. S. Swamy. *Graphs: theory and algorithms*. John Wiley & Sons, 2011.
- [44] Pravin M. Vaidya. Speeding-up linear programming using fast matrix multiplication. In *30th annual symposium on foundations of computer science*, pages 332–337. IEEE Computer Society, 1989.
- [45] P. L. Wong and R. Larson. Optimization of natural-gas pipeline systems via dynamic programming. *IEEE Transactions on Automatic Control*, 13(5):475–481, 1968.
- [46] Aaron C. Zecchin, Angus R. Simpson, Martin F. Lambert, Langford B. White, and John P. Vítkovský. Transient modeling of arbitrary pipe networks by a laplace-domain admittance matrix. *Journal of Engineering Mechanics*, 135(6):538–547, 2009.
- [47] Shixuan Zhang, Sheng Liu, Tianhu Deng, and Zuo-Jun Max Shen. Transient-state natural gas transmission in gunbarrel pipeline networks. *INFORMS Journal on Computing*, 32(3):697–713, 2020.
- [48] Anatoly Zlotnik. Gas reliability analysis integrated library, 2018. <https://github.com/lanl-ansi/grail/>.
- [49] Anatoly Zlotnik, Michael Chertkov, and Scott Backhaus. Optimal control of transient flow in natural gas networks. In *Conference on Decision and Control*, pages 4563–4570. IEEE, 2015.
- [50] Anatoly Zlotnik, Sergey Dyachenko, Scott Backhaus, and Michael Chertkov. Model reduction and optimization of natural gas pipeline dynamics. In *Dynamic Systems and Control Conference*, volume 57267, 2015.
- [51] Anatoly Zlotnik, Line Roald, Scott Backhaus, Michael Chertkov, and Göran Andersson. Coordinated scheduling for interdependent electric power and natural gas infrastructures. *IEEE Transactions on Power Systems*, 32(1):600–610, 2016.
- [52] Anatoly Zlotnik, Aleksandr M. Rudkevich, Evgeniy Goldis, Pablo A Ruiz, Michael Caramanis, Richard Carter, Scott Backhaus, Richard Tabors, Richard Hornby, and Daniel Baldwin. Economic optimization of intra-day gas pipeline flow schedules using transient flow models. In *PSIG Annual Meeting*, pages PSIG-1715. PSIG, 2017.